Accepted manuscript at Deep-Sea Research Part I. doi:10.1016/j.dsr.2017.07.003

Relation of sortable silt grain-size to deep-sea current speeds: Calibration of the 'Mud Current Meter'

I.N. McCave[1*], D.J.R. Thornalley[2] and I.R. Hall[3]

[1] Godwin Laboratory for Palaeoclimate Research, Department of Earth Sciences, University of Cambridge, Downing Street, Cambridge CB2 3EQ, U.K.

[2] Dept of Geography, University College London, Gower Street, London, WC1E 6BT, U.K.

[3] School of Earth and Ocean Sciences, Cardiff University, CF10 3AT Cardiff, U.K.

*Corresponding author: mccave@esc.cam.ac.uk

Abstract.

Fine grain-size parameters have been used for inference of palaeoflow speeds of near-bottom currents in the deep-sea. The basic idea stems from observations of varying sediment size parameters on a continental margin with a gradient from slower flow speeds at shallower depths to faster at deeper. In the deep-sea, size-sorting occurs during deposition after benthic storm resuspension events. At flow speeds below 10-15 cm s^{-1} mean grain-size in the terrigenous non-cohesive 'sortable silt' range (denoted by $\overline{SS}$, mean of 10-63 μm) is controlled by selective deposition, whereas above that range removal of finer material by winnowing is also argued to play a role.

A calibration of the $\overline{SS}$ grain-size flow speed proxy based on sediment samples taken adjacent to sites of long-term current meters set within ~100 m of the sea bed for more than a year is presented here. Grain-size has been measured by either Sedigraph or Coulter Counter, in some cases both, between which there is an excellent correlation for $\overline{SS}$ (r = 0.96). Size-speed data indicate calibration relationships with an overall sensitivity of 1.36 ± 0.19 cm s^{-1}/μm. A calibration line comprising 12 points including 9 from the Iceland overflow region is well defined, but at least two other smaller groups (Weddell/Scotia Sea and NW Atlantic continental rise/Rockall Trough) are fitted by sub-parallel lines with a smaller constant. This suggests a possible influence of the calibre of material supplied to the site of deposition (not the initial source supply) which, if depleted in very coarse silt (31-63 μm), would limit $\overline{SS}$ to smaller values for a given speed than with a broader size-spectrum

supply. Local calibrations, or a core-top grain-size and local flow speed, are thus necessary to infer absolute speeds from grain-size.

The trend of the calibrations diverges markedly from the slope of experimental critical erosion and deposition flow speeds versus grain-size, making it unlikely that the $\overline{SS}$ (or any deposit size for that matter) is simply predicted by the deposition threshold. A more probable control is the rate of deposition of the different size fractions under changing flows over several tens of years (the typical averaging period of a centimetre of deposited sediment). This suggestion is supported by a simple depositional model for which the deposited $\overline{SS}$ is calculated from measured currents with a size-varying depositional threshold. More surficial sediment samples taken near long-term current meter sites are needed to make calibrations more robust and explore regional differences.

Keywords: Sortable silt; current; calibration; mud current-meter; sediment deposition

1. Introduction

Flow in the deep ocean that controls particle transport and deposition on geological time scales, especially under Deep Western Boundary Currents (DWBC), has produced great piles of muddy sediment known as 'drifts', commonly a hundred or more kilometres long and tens wide. These have been exploited by palaeoceanographers because they have sedimentation rates much higher (more than ten times) than the average for the world ocean and thus afford records of past ocean change at enhanced temporal resolution. Because they are produced by flow, they should contain records of variations in the vigour of past deep ocean circulation. The sediments in these bodies are known as 'contourites' because they are deposited from geostrophic currents that flow along topographic contours. There is a burgeoning literature on this topic (see, for example, Rebesco and Camerlenghi (2008) and the > 1400 references therein). Here we present results ot the first field-based calibration showing the relationships between flow speed from current meters and the grain-size of deposited sediment, in particular the mean size of the 10-63 μm terrigenous sediment fraction known as 'Sortable Silt' denoted by $\overline{SS}$ in μm. A calculation of the $\overline{SS}$ grain-size of deposits from examples of measured currents employing a critical deposition criterion is also presented to demonstrate the nature of the controls on size properties of deposited material.

The development of our understanding of the modern deep circulation of the oceans has involved indirect estimates via mapping of the density field, distribution of chemical properties, and direct measurements using current meters and neutrally buoyant floats (Warren, 1981). In contrast the palaeoceanographic 'tool-kit' is more limited. A few attempts have been made to estimate the past vigour of deep circulation via geostrophy with density estimates from oxygen isotopes (Lynch Stieglitz et al., 1999), from the variation in the sedimentary $^{231}Pa/^{230}Th$ ratio (McManus et al., 2004), and many speculations based on the distribution of nutrients and other chemical properties (e.g. Curry and Oppo, 2005; Piotrowski et al., 2004). Several studies have shown changes in the relative vigour of the deep circulation using variations in the sortable silt mean size $\overline{SS}$ (e.g. McCave et al., 1995b; Kleiven et al., 2011, and many others, see Supplementary material #2). The latter approach using grainsize has thus far remained unquantified and it is the purpose of the present paper to provide a quantitative basis for demonstration of the magnitude of bottom current flow speed changes that may be inferred from changes in $\overline{SS}$ This is important for the major changes in ocean circulation that accompanied glacial to interglacial climate shifts, and indeed reconstructions at all timescales, particularly for extending the observational record and integrating with numerical modelling studies.

1.1 Relationship between sediment size and dynamics of the depositing flow.

The size of particles that are moved and deposited has been related to the speed of the responsible flow since at least the time of Sorby's (1859) experimental studies. Most subsequent work related to deposition of sands (> 63 μm) and gravels (> 2 mm), with influential, but misleading, work relating to fine sediments being presented by Hjulstrom (1939; see critique by Dade et al., 1992). Ledbetter and Johnson (1976) pioneered the use of fine sediments as deep-sea current speed indicators, but ascribed the size variations to winnowing removal of particles rather than control by deposition as advocated by McCave and Swift (1976).

As particles increase in size they become less prone to aggregation and aggregates are more easily broken up by turbulent stresses. For most fine sediments the disaggregated state in which the samples are analysed is not the state in which they were deposited, because that involved varying degrees of particle aggregation. Therefore dynamical inferences may not be made from the properties of the whole size distribution down to clay size. Only terrigenous sediment is considered because biogenic particles (coccoliths, diatoms etc) are created at particular sizes which could bias a measurement of material to be interpreted as resulting from current-controlled sorting. In addition the percentage of clay may depend on whether the source area is heavily chemically weathered, yielding much clay. This fact led McCave et al. (1995a) to propose the use of the 10-63 μm silt fraction, which they called 'Sortable Silt' (as distinct from cohesive silt of 2-10 μm size), as a flow speed indicator because the grains were more likely to have been deposited individually, controlled by local fluid stress and their settling velocity.

Sediment size-sorting occurs principally during resuspension and deposition by processes of aggregate break-up and particle selection according to settling velocity (w_s) and fluid shear stress (τ). Controlling variables are critical stresses that just permit erosion (τ_e), suspension (τ_s) and deposition (τ_d). In general $\tau_d < \tau_e < \tau_s$ for non-cohesive material. In what follows, use is also made of the shear velocity $u_* = (\tau/\rho)^{½}$ where ρ is fluid density. Under a given stress some grains and aggregates are deposited, while others of smaller settling velocity are kept in turbulent suspension and transported further down current. Sorting of fine-grained deep ocean muds thus arises mainly from selective deposition (Mehta and Lott, 1987, McCave et al., 1995a). Selective erosion of finer components (*winnowing*) can make a deposit somewhat coarser overall by producing intermittent erosion horizons marked by a coarse silt–sand lag, which is then biologically mixed into the deposit (almost all deep-sea sediments are bioturbated). These arguments have been set out in greater detail by McCave and Hall, (2006) and McCave (2008a).

The sorting process is thought to be event-driven, the events being deep-sea storms producing sediment suspensions and their depositional consequences (Gardner and Sullivan, 1981; Hollister and McCave, 1984; Gross and Williams, 1991). These resuspension events are relatively short-lived, contributing the high tail to flow speed spectra, and the intervening long periods of slow depositional flow dominate the mean flow speed record and control the grain-size of the accumulated material.

1.2 Field and Laboratory previous work

Ledbetter (1986) presented a field calibration of a 'silt-mean size' parameter using current meters deployed along the axis (and far above the bottom) of Vema Channel (S.W. Atlantic), though many of the sediment samples were not close to the current meters in mid channel as they were collected from the channel flanks at a similar depth. The 'silt-mean size' was the moment mean calculated from Elzone particle counter data in the range 4.8 to 62.5 μm (7.7 – 4.0 φ, where $\varphi = -\log_2 d$ (in mm)). This includes a large fraction of cohesive silt material from ~4.8 -10 μm. The Ledbetter (1986) data give a relationship between silt-mean size and the scalar flow speed (U) of $dd/dU = 0.45$ μm /cm s^{-1}, with r = 0.911 (Fig. 1. New determinations of the grainsize ($\overline{SS}$) of many of Ledbetter's samples by Coulter Counter (CC) are shown together with data from the original publication in Fig. 1. The new data give a slope of $dd/dU = 0.49$ μm /cm s^{-1}, with r = 0.84, quite similar to the original relationship.). The data here and elsewhere in this paper are fitted with a Reduced Major Axis (RMA) (Miller and Kahn, 1962, p. 204). In this the slope of the line is the ratio of standard deviations of x and y, passing through mean x and y. This is used either when there is no dependent-independent relationship, or when the assumption underlying simple linear regression that x is measured without significant error is invalid. In the present case the overall errors in U are large, at least as large as those in $\overline{SS}$ (see section 2.5), and for that reason we use an RMA

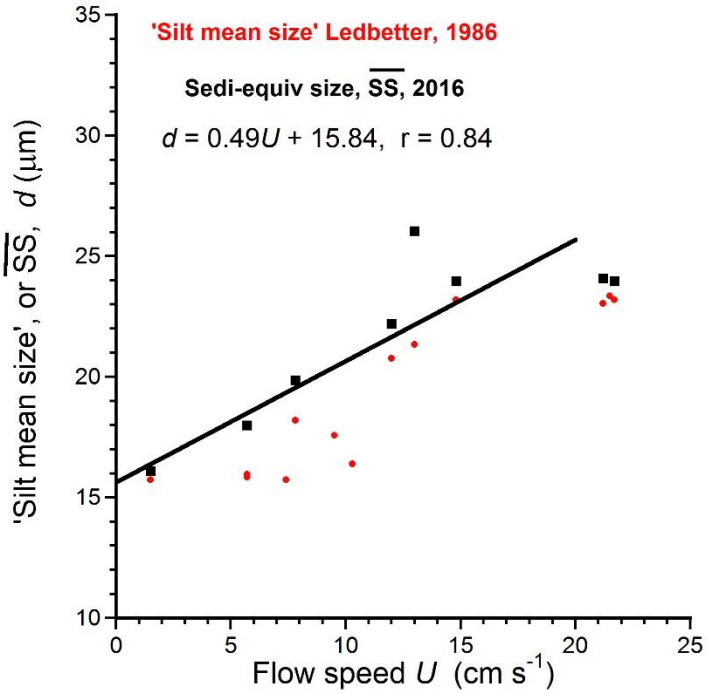

Fig. 1. *Mean particle size data of Ledbetter (1986) from Vema Channel (red dots) and available samples re-analysed by Coulter Counter (expressed as Sedigraph-equivalent' (Sedi-equiv') size* $\overline{SS}$*, see Fig. 2) (black squares) showing reduced major axis (RMA) relationship between mean current speed and particle size parameters (*$\overline{SS}$ *for the 'Sedi-equiv' size, 'silt mean size' for Ledbetter's original data) of the non-carbonate silt fraction.*

In the laboratory Mehta and Lott (1987) observed that under decreasing flow a graded suspension of kaolinite deposited coarser particles. Steady state suspended concentrations (C_{eq}) were reached under slower flow speeds where the remaining suspensions contained finer particles that did not deposit. Thus a series of (C_{eq}/C_0, where C_0 is initial concentration) values were obtained as flow was reduced in steps. They developed an expression for the sorting that is essentially an expansion of the Krone equation (Krone, 1962; Einstein and Krone, 1962) for change in concentration with time t,

$$C_i/C_o = \exp(-w_{si}\, t\, (1-\tau_o/\tau_{ci})\, /D)$$

including several size classes where τ_o is the steady state shear stress and τ_{ci} is the critical depositional stress for a size class, w_{si} is its settling velocity, and D is flow depth. These experiments gave a strong indication of size sorting via selective deposition. However, recent experiments with 13-44 μm silt (mean 30 μm) by Hamm and Dade (2013) found no sorting effect and the deposit size remained the same under a range of shear stresses.

It is also commonly assumed that the size of material on the sea bed is controlled by the critical deposition stress, the stress below which material of a given settling velocity will be deposited. There

has been much work on the critical erosion conditions for fine sediments, mostly with cohesive materials (e.g. Migniot, 1968; Amos et al., 1992; Winterwerp et al., 2012). White (1970) and Mantz (1977) extended the *non-cohesive* critical erosion curve down to the equivalent of 5 μm in water through experiments with a high viscosity fluid (oil). McCave and Swift (1976) argued that the critical depositional stress was approximately equal to the critical erosion stress because it was presumed that, if there was no movement of sediment in the viscous sub-layer, the concentration gradient would reverse and deposition would ensue. This was based on the assumption that once moved, fine particles would be ejected from the viscous sub-layer into full suspension. However, the experiments of Self et al., (1989) in a laminar flow cell showed that the start and end of particle movement were distinct with a stress gap between them. A stress gap between erosion and full suspension was also demonstrated by Nino et al. (2003). At a grain-size of 38 μm the latter authors give the difference in u_* from 0.82 cm s^{-1} for erosion to the very high value of 2.15 cm s^{-1} for full suspension. Further calculations relating to deposition are given in McCave (2008a)

2. General calibration strategy and methods

The overall calibration strategy adopted here has been to obtain and analyse the $\overline{SS}$ grain-size of surface sediment samples (top 1 cm) from as close as possible to the site of long-term (> ~1 year) current meters set at a height in the water column to record a speed approximating that of the geostrophic flow (ideally 30-100 meters above bottom, mab).Collection of sea-floor sediment samples was by several methods, multicorer, box corer, and a small gravity corer suspended below a water bottle rosette frame. The topmost 1 cm of recovered sediment was removed from each core and kept moist prior to laboratory disaggregation, and removal of biogenic carbonate and opaline silica (see McCave et al., 1995a for analytical methods). No samples had high organic Carbon making a further removal procedure unnecessary. Sampling locations are given in Table 1 and shown on maps in Supplementary Information item 1

2.1 Sediment size distributions.

There are natural breaks in the global spectrum of sediment size that reflect the origin and mineralogy of particles (Smalley, 1966; Pettijohn, 1975, p. 40-45). One such break is at the coarse silt/fine sand boundary, in the region 50-75 μm. Different disciplines (engineers, soil scientists, geologists) pick the boundary at different points in this range, but here we use the geologists' 63 μm

as the upper size limit for silt. Clay, defined as either < 2 or < 4 μm, dominantly comprises clay minerals produced by chemical weathering. At these sizes the forces of particle attraction outweigh the particle mass, so sediments are cohesive (Dade et al., 1992). Driscoll et al. (1985) and McCave et al. (1995a) observed that size frequency curves of sediment deposited from deep-sea currents often display a natural minimum around 8-10 μm which they suggested represented the boundary between cohesive/non-cohesive behaviour. This has recently received support from Mehta and Letter (2013) who compiled experimental evidence and concluded that the upper boundary for cohesion lies at 7.4-8.7 μm. However, Law et al. (2008), using a simplified model, noted that "Modeled mobilities using 16 μm as the minimum size for sortable silt are closest to observations." Maybe the widely used 10 μm, as assumed in $\overline{\text{SS}}$ is a satisfactory, but arbitrary, compromise. Law et al. (2008) also noted that when there is more than approximately 7.5 wt% clay in a bottom sediment all sizes are equally mobile, i.e. there is no sorting on erosion. Nearly all deep sea sediments contain at least that proportion of clay.

2.2 Particle size measurements

Particle size measurements were made by either by Coulter Counter (Beckman Multisizer III) or Sedigraph 5100, in several cases both instruments, after opal and carbonate removal by the methods outlined in McCave et al. (1995a), with > 2 day's disaggregation in an end-over-end shaker and 3 min ultrasonic treatment. The Sedigraph works on the classical principle of settling velocity related to particle size by Stokes' Law. Variation in the concentration of a settling suspension is sensed as a function of time by the attenuation of a collimated X-ray beam passing through the suspension. This allows the settling velocity and thus size distribution to be inferred as equivalent spherical diameters assuming a single particle density (Coakley and Syvitski, 1991). In contrast the Coulter Counter works on the principle of counting and sizing particles by volume yielding a volume-frequency distribution (Milligan and Kranck, 1991). Particles are suspended in an electrolyte and drawn through a small aperture where they displace their volume of electrolyte causing impedance changes, which are sized and counted. For all Coulter Counter measurements reported here a 200 μm aperture tube (optimal for size range 2-80 μm) was employed, and three runs of 20,000 particles counted in the 10-63 μm range were averaged. The Sortable Silt mean size ($\overline{\text{SS}}$) flow speed proxy is calculated in the normal sedimentological convention on log-transformed weight (or volume) frequency size of the 10-63 μm range (Krumbein, 1938).

Recent improvements to Coulter Counter technique involving faster stirrer speeds (Moffa-Sanchez et al., 2014) have been applied, though we used a speed setting of ~36 to avoid bubble

entrainment. There is very good agreement between the $\overline{SS}$ estimates by Sedigraph and Coulter Counter (Fig. 2). Data here have been plotted as Sedigraph or if determined by Coulter, Sedigraph-equivalent size using the correlation equation shown on Fig. 2).

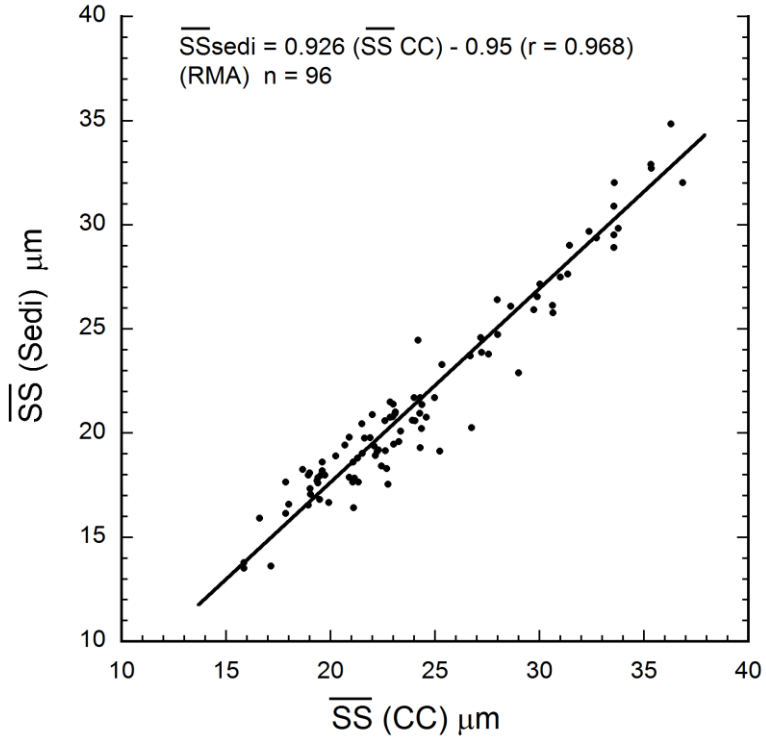

Fig. 2. *Comparison of samples analysed for sortable silt mean size by Sedigraph (Sedi) and Coulter Counter (CC). A Reduced Major Axis is shown because significant errors are present in both axes. In this paper sizes are expressed as 'Sedigraph equivalent' using the equation shown. Conversion from Sedigraph to Coulter counter is via* $\overline{SS}$ *(CC) = 1.08* $\overline{SS}$*sedi + 1.026*

2.3 Speed, not velocity: what speed?

The scalar geostrophic flow speed U_g is used here as this produces the drag that affects the sediment, irrespective of direction. The directional stability may be expressed by the ratio between the mean velocity (vector) and speed (scalar).

In the analysis of current meter flow speeds to be correlated with grain-size, two arguments are possible. One is that because the material analysed is finer than 63 µm, only flow speeds that would permit deposition of material below that size should be admitted to calculation of the mean speed for correlation purposes. Critical erosion experiments and observations tell us that when current speeds are sufficient to move sand they remove finer sizes and leave a sandy lag (> 63 µm, generally foraminiferal sand in the deep sea) that is commonly rippled (Miller and Komar, 1977; McCave et al., 1980). For < 63 µm material, assuming smooth flow for the skin friction component (yielding a thick

enough viscous sublayer to control deposition, and ignoring the form drag of biogenic roughness), critical depositional shear velocity u_{*d} is < ~0.67 cm s^{-1} (Self et al., 1989. Using the drag relations of Csanady (1972), $u_* = U_g/30$ or Bird et al. (1982), $u_* = U_g/27$, this gives flow speeds U_g = 20.1 to 18.1 cm s^{-1} for the critical depositional velocity. An upper limit might be given by the critical erosion shear for the sand-silt boundary of 63 μm which under deep sea conditions (T ≈ 2°C, ρ ≈ 1050 kg m^{-3}) is u_* = 0.96 cm s^{-1} (Miller et al, 1977) or U_g = 26 - 29 cm s^{-1}.

The alternative view is that no selection of allowable speeds should be made. This is because the velocities above critical deposition speed may erode finer material and leave behind a coarser deposit than would be the case if there were no high speed component to the flow speed spectrum. Although initially in thin lag layers, biological mixing ensures that the coarse-tail signature is spread through a 1-cm thick sediment sample at time scales considerably faster than accumulation. In such a case the mean of the flow speed record without truncation should be taken. The objection to using the speeds > 0.25 m s^{-1} is that the bulk material < 63 μm which contains clay tends to be cohesive and is not eroded grain-by-grain, thus the higher speeds do not sort these particles by primary size on erosion (Amos et al., 1992; Dade et al., 1992; Mitchener and Torfs, 1996; Law et al., 2008). Nevertheless several authors have demonstrated size-dependant erosion of fine sediment in field and laboratory experiments (Drake and Caccione, 1986; Wheatcroft and Butman, 1996; Teeter et al., 1997). We choose to be inclusive so the case of the untruncated flow speed spectrum is examined here.

A further problem raised by McCave et al. (1995a) is whether the particle size characteristics are determined by the mean flow or its variability, i.e. whether mean (K_M) or eddy kinetic energy (per unit mass) (K_E) is dominant. Conventionally K_M and K_E are based on the resolved east (u) and north (v) components of velocity: $K_M = 0.5(U^2 + V^2)$ and $K_E = 0.5(u'^2 + v'^2)/n$, where $u'^2 = \Sigma(u - U)^2$ and similarly for v', where u, v are the instantaneous values and U, V are the record-length means (Dickson, 1983). However in the present case where the scalar speed (S) is employed, $K_M = 0.5(S)^2$, $K_E = 0.5[\Sigma(s - S)^2/n]$, where S is the record-length mean speed, s the instantaneous (hourly or half-hourly (as available) speed and n the number of observations. Thus K_E is simply half the mean square value of the deviations s' from the mean S, or the variance of the speed. Current meter data are taken mainly from the WOCE database (http://ewoce.org/data/index.html) or via the WOCE Current Meter Data Assembly Center operated by Oregon State University (http://kepler.oce.orst.edu/). Hourly or half-hourly speeds have been used here (Table 1).

In adopting this approach we do not loose sight of the fact that the last major event of dynamical significance that occurred to the sediment was that it was deposited, and that depositional,

not erosional, conditions are of paramount importance for fine sediments, where, as Dyer (1986, p.vii) so perceptively observed, "*…there are large areas of the sea bed where the sediments are cohesive until they are moved, and are non-cohesive until they are deposited.*" Where erosional conditions dominate, the resulting sedimentary records tend to have a slow accumulation rate and lack high stratigraphic resolution and thus are typically avoided for paleoceanographic studies.

2.4 Current meter height in the benthic boundary layer (BBL)

In order to provide a $\overline{SS}$ calibration what we seek is a measurement that approximates the geostrophic velocity U_g, i.e. a flow speed uninfluenced by proximity to the seafloor boundary. The Ekman layer thickness $H_E = (\kappa u_*/f)$ or ~ 4000 u_* with the mid-latitude Coriolis parameter $f \sim 10^{-4}$ and von Karman's constant $\kappa = 0.4$. The u_* values given above for critical erosion and deposition conditions would give Ekman layers typically 25-50 m thick. However modelling does not normally give the thicknesses recorded by Armi and Millard (1976) with thermistors, or optical systems recording the bottom mixed nepheloid layer which can be up to 100 m thick (Eittreim et al., 1969; Armi and d'Asaro, 1980; Spinrad and Zaneveld, 1982; McCave, 1983, 2008b). We conclude that U_g may reasonably be taken to be that above 30-100 mab, below which the flow is frictionally influenced by the boundary. We therefore need to make an upward adjustment for flow speeds recorded below ~30 mab (m above bottom) to make them comparable with those from 30 - ~ 100 mab. In the case of several records from the S. Iceland slope where meters were at 10 mab, while others were at 50 mab, a factor of 1.08 based on the velocity profile of Bird et al. (1982) has been applied to obtain speeds at ~50 mab. In general we have excluded meters from more than 120 mab as not necessarily providing speeds that relate to the stress felt at the sea bed.

2.5 Errors: Flow speed

The variability of flow speed in a current meter record can simply be represented as the standard deviation of the values of speed. (Some authors average a logarithmic transform because speed records are often highly skewed). For one of our records, for example (W1, 2005-6), mean speed is $\bar{U}$ = 6.77 cm s^{-1}, 2x standard error (SE) = 0.092 cm s^{-1}, a mere 1.36%. But that gives too rosy a view of the variability because the number of observations is very large (thus SE = $\sigma/\sqrt{n}$ is small). We have in many cases only one or two years data, and variability over the longer term which would match the multi-decadal integration time scale represented by the 1 cm of sediment from a core top is unknown. The best we can do is to examine the few records where we have several years data to assess inter-annual variability. Data from three sites on Line W for 4 years (Table 1) have an average

of (2SE/mean) as a percentage equal to 11.8%. But it may be objected that this SE is based on just 4 annual mean values. A simple alternative is to take half the range of the 4-years of mean values as a percentage of the mean speed and regard that as the ± error, which for these sites is 12.7%. On Figure 3 the U axis error is shown as ± 12.5% at 10 cm s^{-1}. (For current meters at a site in Rockall Trough with greater directional stability (SMBA1800) for only 2 years of deployment the 2SE/mean is just 0.69% and 0.5 of the interannual range is 4.1 cm/s on a mean of 15.7cm/s, so the value of 12.5% adopted is very conservative)

2.6 Errors: Sediment size

The analytical uncertainty in $\overline{SS}$ measurement have been set out by Bianchi et al. (1999) where the errors for Sedigraph and Coulter Counter are ± <3% when amount of SS is >5%. That would give an error of ±0.6 μm at 20 μm. However, we must also ask how representative is one sample in the vicinity of the current meter mooring: how large is the uncertainty due to spatial variability? In a precursor study to development of the notion of the Sortable Silt proxy, McCave (1985) showed that a coarse silt modal size was well correlated with the height of that mode, more or less equivalent to correlation of $\overline{SS}$ and SS%. Data from the top 5 mm of 23 box cores positioned in a 2x4 km area gave a mean coarse mode size of 14.55 μm with 2SE of 0.69 μm, or mean ± 4.74%. The combined measurement and spatial uncertainty by error propagation (2SE) is thus ± 5.6% (Fig. 3).

Rather than plot each point with ± 12.5% in x (*U*) and ± 5.6% in y ($\overline{SS}$), representative error bars are shown on Fig. 3 as the exact errors for each speed and size record are unknown.

2.7 Some challenges associated with the existing current meter dataset

None of the current meter arrays potentially available for use in this study were deployed with $\overline{SS}$ calibration in mind and therefore present a range of difficulties for this purpose. Physical oceanographers quite reasonably tend to set their meters in locations where the greatest signal, i.e. largest current speed, will be recorded so as to give the best estimates of water flux. Unfortunately, for paleoceanographic purposes these conditions often cause sea bed erosion, thus no usable sediment record. Additionally, some meters have been set in inappropriate locations for our purposes such as WOCE line ICM3 along 20°S off Madagascar laid adjacent to a turbidity current channel (with one meter in the channel, but right on 20°S). Here the sediment was coarse micaceous sand from the island's granites delivered by high speed gravity flows rather than mud reflecting geostrophic current-influenced deposition. At this location Warren et al (2002) lamented that a dominant bimonthly oscillation (of Rossby wave origin) was "a great disappointment because it obliterates a portion of the

mean flow that the current-meter array was put out to measure". Other current meter sites off Greenland and Labrador proved to be in ice-rafted boulder fields. Many current meter arrays have no meter close to the bed, or meters in the 20 to 120 mab range gave no record, so coring at these sites was avoided.

3. Results.

3.1 Silt mean - flow speed correlation

$\overline{SS}$ is plotted as $f(U)$ in the plot in Fig. 3 where it is immediately seen that points can be grouped along several sub-parallel lines. We start from the point that there is a line well-defined by 9 points for the Iceland overflow region ($\overline{SS} = 0.762U + 16.18$, r = 0.932). Guided by this, several other lines can be recognised. It can also be seen that, strangely, some of these groupings involve points from quite different sedimentary systems, which might lead one to question their validity were it not for the fact that even when split apart the lines for the two data sets are sub-parallel (Table 2). This is the case for deep Line W/Rockall, Weddell/Scotia, and ACM6 (Atlantic Current Meter line 6) and S Iceland. There is a well-defined line with a slope $d\overline{SS}/dU = 0.81$ μm /cm s^{-1} containing 12 calibration points ('main line'), 9 of which are from the Iceland overflow region. All of these points are from water depths shallower than 2400 m and are close to their sediment source. The 3 additional points defining the line come from the Grand Banks Slope (ACM6 meters at 1.5 and 3.25 km) and Portuguese slope at 1.3 km. The five data points from line W south of Woods Hole, NW Atlantic, fall into two groups (i) a group of three points from sites deeper than 3.2 km on the continental rise under the DWBC and (ii) two points from higher up the continental slope at depths shallower than 2.7 km. Three points from the deeper part of the western side of Rockall Trough (BENBO sites A and C and RAPiD-01-1B/SMBA1800) some

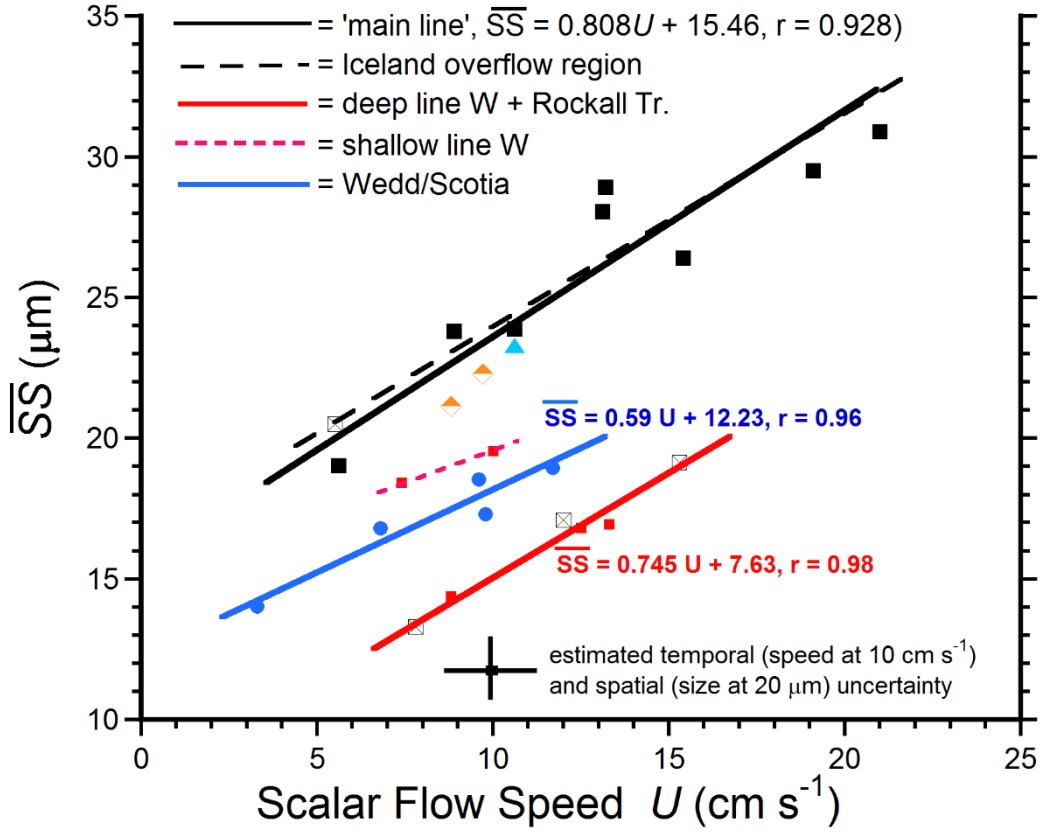

Fig. 3. *Data from current meters and nearby sediment samples plotted as* $\overline{SS} = f(U)$. *See Table 1 for locations and data. The heavy black line is the 'main line' referred to in the text. Lines are Reduced Major Axes. The RMA is inverted to* $U = f(\overline{SS})$ *to give an equation for prediction of speed from grain-size whose slope is the sensitivity. The various lines are discussed in the text. Most points are colour-coded with their lines but orange and blue triangles are ACM6 and Morena respectively, and boxed Xs are BENBO and Rockall Trough sites (see Table 1),*

way from their sediment source on the Irish/Scottish margin plot close to the Line W points. The latter line has a slope close to that of the 'main line' with $\overline{SS} = 0.745U + 7.63$. Another line is defined by five points from N and S of the Antarctic Peninsular in the Scotia and Weddell Seas, at 2850 - 4570 m water depth. Again these are perhaps fortuitous bedfellows as Weddell sites lie under a DWBC while the Scotia Sea sites are under the Antarctic Circumpolar Current (ACC), but the fact that they have a similar source off the E and W sides of the Antarctic Peninsular may allow us to group them. Their line with $\overline{SS} = 0.515U + 12.73$ is also sub-parallel to the 'main line'. Considering the error estimates for U_g and $\overline{SS}$ the implied sensitivity in the latter case is statistically within error of that for the 'main line' (see sections 2.5 and 2.6 for assessment of errors).

Taken at face value (i.e. ignoring the uncertainty), these data suggest the influence of a deficit of coarse silt (thus finer mean size for the same speed) at the deeper sites on Line W and the Scotia/Weddell Sea**,** relative to those where sites are closer to supply source from the shelf in the area south of Iceland and the shallower part of Line W. Two explanations are possible, first that the sediment supply does not contain as much coarse silt in these areas as in the south Iceland rise region, or second that the supply of coarse silt has been depleted by deposition further upstream along the deep current flow path (progressive down-current fining). The similarity of Rockall and deep line W may thus be seen as possibly reflecting a similar position along their transport paths away from source. Such a fining was discussed by Haskell and Johnson (1993) and McCave and Hall (2006) and can be seen in the data of Bianchi and McCave (2000) along Gardar Drift south of Iceland. This will make it difficult to define a universal conversion from $\overline{SS}$ to absolute flow speed unless there is a local calibration such as for the Iceland overflow region (as utilised by Thornalley et al., 2013a), deep Line W or the Scotia Sea, but the apparent constancy of the slope, i.e. the *sensitivity* (cm s^{-1}/μm, see section 3.2), means that the scale of absolute *changes* in flow speed could be estimated with some confidence at a given location.

3.2 Sensitivity

The physical relationship is $\overline{SS} = f(U)$ and that is how it is plotted in Fig. 3. The sensitivity is the inverse of this, $dU/d\overline{SS}$ cm s^{-1} per μm. The slopes of the three principal groups of points on Fig. 3 are 0.808 ('main line'), 0.745 (Line W/Rockall) and 0.515 (Weddell/Scotia) (Table 2). The similarity of these slopes, considering the error estimates of ± 5.6% in $\overline{SS}$ and 12.5% in *U*, suggests that they can be represented by a single value. One simple approach is calculation of the weighted mean slope value which,

Table 2 Slope data for lines fitted to $\overline{SS}$ and *U* data by RMA

	data set	$d\overline{SS}/dU$	sensitivity cm s^{-1}/μm	Eq. Const	n	r	weighted slopes	sensit[y]
	Aggregated sets							
1	Main line	0.808	1.238	15.46	12	0.928	9.696	
2	W Deep + Rockall	0.745	1.342	7.63	6	0.980	4.470	
3	Weddell + Scotia	0.515	1.942	12.73	5	0.960	2.575	
	Individual sets				23	0.949	0.728	1.374
1	Iceland Overflow reg[n]	0.762	1.312	16.18	9	0.932	6.858	
2	W Deep	0.602	1.662	--	3	--	1.805	
3	Rockall	0.790	1.266	--	3	--	2.369	
4	Scotia	0.515	1.941	--	3	--	1.545	

5	Weddell	0.505	1.982	--	2	--	1.009	
6	ACM6	1.267	0.789	--	2	--	2.535	
7	W Shallow	0.979	1.022	--	2	--	1.957	
	We do not generate an r value for 3 or fewer points				24		0.753	1.328

Based on U/<U> vs $\overline{SS}$/<$\overline{SS}$> normalisation, 25 points

SE of slope is $(sy/sx)((1-r^2)/n)^{0.5}$	$d\overline{SS}/dU$	$dU/d\overline{SS}$	r^2	SE	2SE
	0.736	1.358	0.880	0.094	0.188

inverted, gives the sensitivity. Two ways of doing this are shown in Table 2; (i) a weighted average of the three aggregated data sets where different sedimentary systems are summed together ($dU/d\overline{SS}$ = 1.374), and (ii) a weighted average of all the slopes of the individual data sets ($dU/d\overline{SS}$ = 1.328). Both have unappealing features; in i) different systems are grouped (Weddell + Scotia, LineW + Rockall), while in ii) standard deviations are calculated for 2 and 3 points. An alternative is to plot the $\overline{SS}$ and *U* normalised by the mean for each data set as shown in Fig. 4, from which the slope (sensitivity) can be obtained. This yields a value of 1.36 ± 0.19 cm s^{-1}/µm (±2SE error). For results from a Coulter Counter the sensitivity is 1.47 ± 0.20 cm s^{-1}/µm (using the slope of Fig. 2).

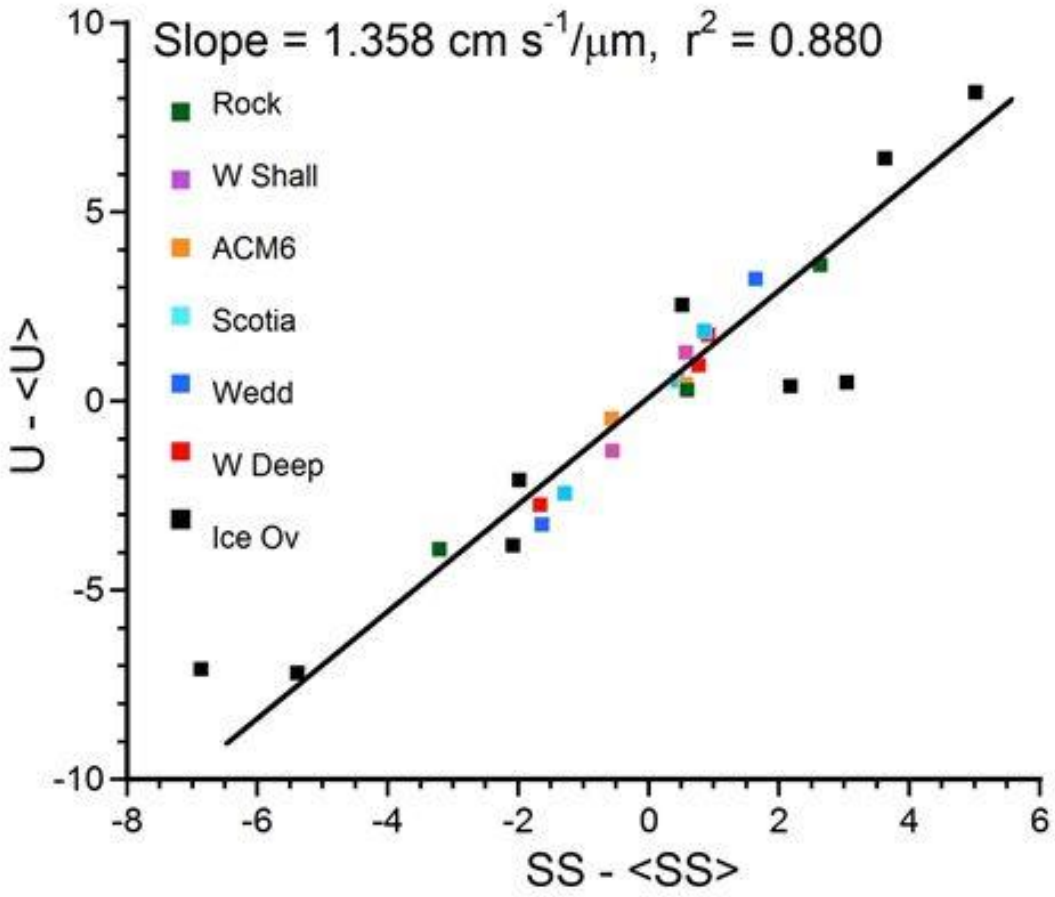

Fig. 4. *Normalised* $\overline{SS}$ *versus normalised U for the three principal groups of data in Fig. 3 with points coloured as the lines as in Fig. 3. The line is an RMA. Sensitivity is 1.36 ± 0.19 cm* $s^{-1}/\mu m$*. Data colour codes are for Rockall, Line W shallow, ACM6, Scotia Sea, Weddell sea, Line W deep and Iceland overflow region.*

This is an important result for palaeoceanographic flow speed reconstructions in that, while the absolute speed may not always be calculable, the magniture of *absolute changes* in flow speed can be estimated with a good degree of confidence. This continues to hold in cases where the whole data set is shifted to sizes finer than the 'main line' (and an absolute speed can be estimated). The original and rerun results of Ledbetter (1986) also have a steep slope, resembling results of the present data sets, lending some confidence to the clear difference from the trend of a critical deposition prediction (Fig. 7B, see sect. 4.3).

A number of recent studies have used laser particle sizers, but the relationship between them and other instruments is less well defined. The principal instruments currently in use are the Beckman Coulter LS 13 230 (e.g. Jessen and Rasmussen, 2015; Li and Piper, 2015), the Malvern 2000 series (e.g. Andrews et al., 2016) and the Fritsch Analysette (Jonkers et al., 2015). Each uses a different algorithm to invert the angular distribution of forward-scattered light intensity to an equivalent spherical diameter size distribution. While their use may be reasonable for palaeocurrent reconstructions, it cannot be assumed that the relationship is identical and therefore specific laser to Sedigraph or Coulter counter intercomparisons will be required to utilise the $d\overline{SS}/dU$ calibration presented in this study.

3.3 Correlation of $\overline{SS}$ *grain-size and percentage abundance*

A fairly well-known result is that the $\overline{SS}$ grain-size and the percentage abundance of sortable silt (*SS%*) within the total <63 μm fraction are well correlated McCave and Hall (2006). Figure 5 shows this for over 1500 data points where two principal datasets have differing trends but nevertheless an overall close correlation. The significance of this is that a greater proportion of sortable silt (*SS*%) corresponds to coarser $\overline{SS}$. The explanation for this given above is that under a stronger

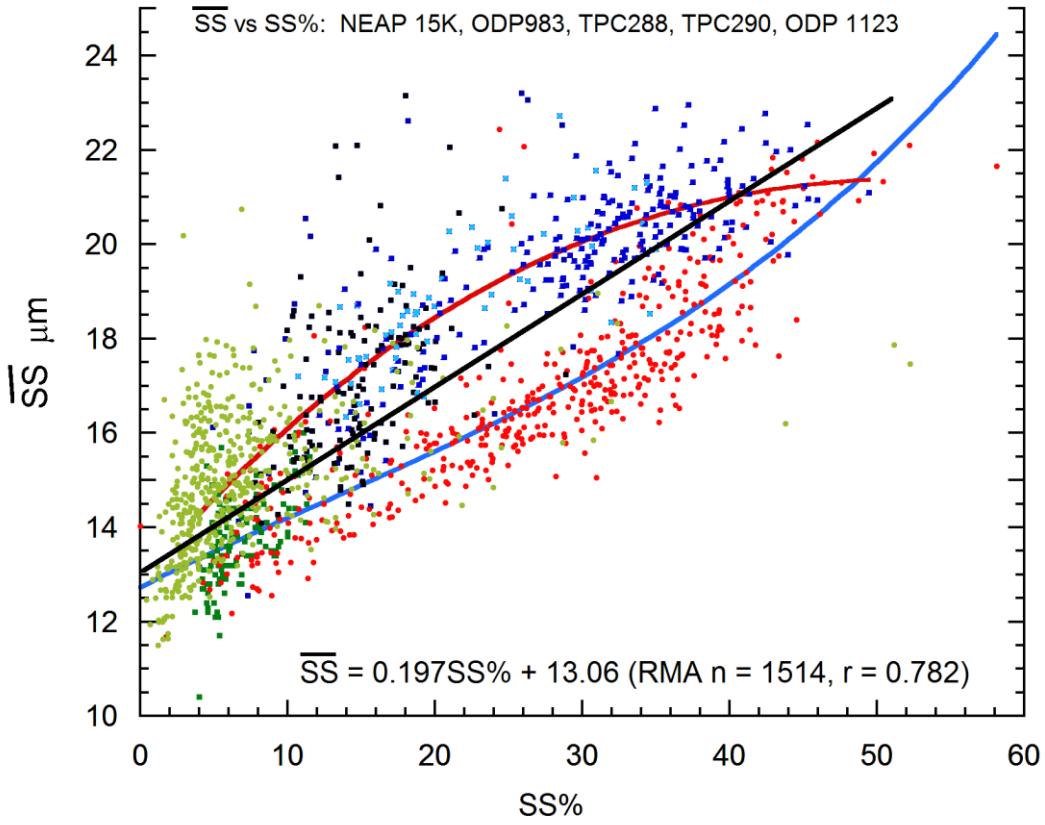

Fig. 5. *Sortable silt mean size versus sortable silt percentage; [%(10-63)/< 63]. All data are in the linear fit, and the two principal data sets (blue points, Scotia Sea, r = 0.795 (Pugh, 2008); red points N. Gardar Drift, r = 0.880 (Kleiven et al, 2011)) have cubic fits. Green is ODP 1123 (Hall et al., 2001). The 13 data points which have SS% values from the present calibration set are very well behaved in this regard, close to the average fit, with a line of slope 0.208, intercept 13.64 and r = 0.926). Similar good behaviour is recorded for measurements by laser sizer (Supplementary Information, Sect. 3).*

current the deposition of fine sediment is suppressed in the fine tail of the sortable silt range and therefore the proportion of sortable silt in the total fine fraction (<63 µm) increases and as a result the $\overline{SS}$ also increases. These features were shown by McCave (1985) in a suite of box core tops from a small area where the coarse silt mode abundance was positively correlated with its size (the data set used to assess spatial variability). In addition the size of the coarse mode was negatively correlated with the percentage of clay. These data were from the top 0.5 cm of the seabed and, being from a small area, have the same source and upstream history. This argues against the possibility that the correlation between range of silt mean size and percentage is due to varying source during glacial and

interglacial changes in the North Atlantic and Southern Ocean as represented by the datasets in Figure 5.

3.4 K_E versus K_M

The correlation between the $\overline{SS}$ and eddy kinetic energy for the twelve calibration points falling on the 'main line' do not suggest a strong role for K_E (Fig. 6), but it is in the nature of the sites selected for current meter deployment and sediment sampling that a strong unidirectional signal should be detected, i.e. dominant K_M. It is also the case in the present data mainly from DWBCs that K_E and K_M are positively correlated ($r^2 = 0.464$), so the weak correlation in Fig. 6 between $\overline{SS}$ and K_E is not unexpected.

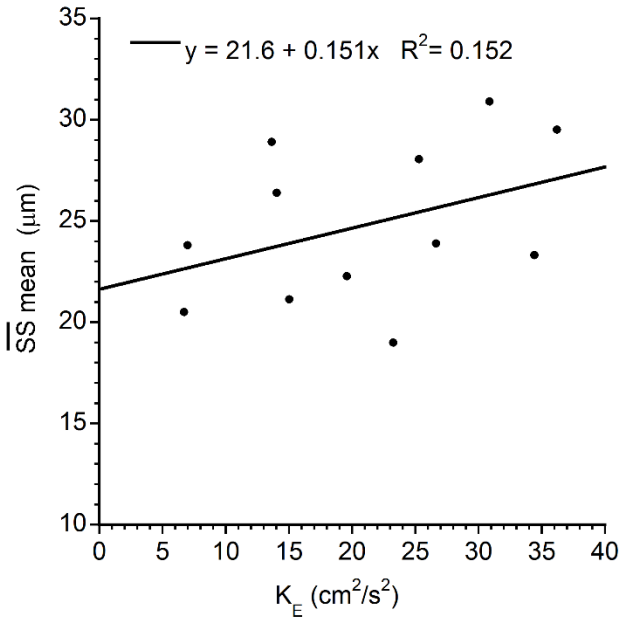

Fig. 6. *Sortable silt mean size versus eddy kinetic energy for the 12 points on the 'main line' of Fig. 3. A weak positive correlation is apparent.*

4. Discussion

4.1 Possible source effects.

It is proposed here that the offsets to finer sizes shown by the Line W (northwest Atlantic), Rockall (NE Atlantic) and Weddell/Scotia data sets are due to a dearth of coarse silt resulting from its removal by deposition further upstream in the transport system. It is regarded as unlikely that the difference stems from an original deficit of coarse silt in the primary source population. This is borne out by the Line 'W' data for the two shallower slope sites, where a more direct input of sediment from the shelf edge is expected, that come closer to the 'main line'. The main group of deep Line W

calibration points are from sediments supplied along slope by the Western Boundary Undercurrent (WBUC) that are obtained from turbidity current deposits on the Laurentian Fan. The signature of this is found in the 'rose-gray lutites' of Hollister and Heezen (1972) found all along the eastern U.S. continental margin. Other reasons why direct source effects are likely unimportant have been set out by McCave and Hall (2006). They include the fact that most sediment is delivered to the deep sea by gravity flows which mix substantial thicknesses of failed seabed resulting in elimination of effects due to systematic temporal variability of sources (e.g. climatic) on at least short timescales (order of at least 100 ka, maybe to 1 Ma) (Talling et al, 2013; Weaver and Thomson, 1993).

The offsets to the $\overline{SS}$ *vs SS%* relationships shown in Fig. 4 could be interpreted to suggest possible source effects in that the Scotia Sea sediments, although current-driven, have an ice-rafted debris (IRD) input, whereas the Gardar Drift site is mainly supplied by currents transporting material from the S. Iceland slope. However, both data sets cover interglacial and glacial (with IRD) conditions so the difference cannot be attributed to IRD input. In the Scotia Sea the $\overline{SS}$ sensitivity is reduced at larger *SS%* (>~25%) but at Gardar Drift the sensitivity of the $\overline{SS}$ is maintained throughout the range of *SS%* (5-50%). From this contrast one could infer a limitation of coarse silt supply in the Scotia Sea. Although this does not accord with generally erroneous presumptions regarding the effect of IRD addition on $\overline{SS}$, the data of Andrews and Principato (2003, see Supplementary material #5) show that in most cases in the glacial sediments of Ross Sea and off E. Greenland there is an excess of fine over coarse sortable silt. Addition of IRD, if unsorted, is thus not very likely to result in coarser $\overline{SS}$.

4.2 Disagreement with theoretical depositional stress/speed

Both the critical deposition and critical erosion curves are rather flat (moderate variation in *U* over the $\overline{SS}$ range), with a gap between initial movement and deposition (McCave and Swift, 1976; Self et al., 1989) in terms of flow speed versus size (Fig. 7A). The variation in shear stress implies an increase of less than a factor of 2 in flow speed over this range. The same is true of the critical deposition condition (Self et al., 1989). The calibration given here (Fig. 3 & 4), however, suggests much greater sensitivity of deposited $\overline{SS}$ to flow speed. It also indicates substantial disagreement with the notion that the critical thresholds for either deposition or erosion directly and solely control the mean size of the deposited <63 μm sediment fraction. In the following we therefore attempt to model the size of sediment deposits resulting simply from selective deposition.

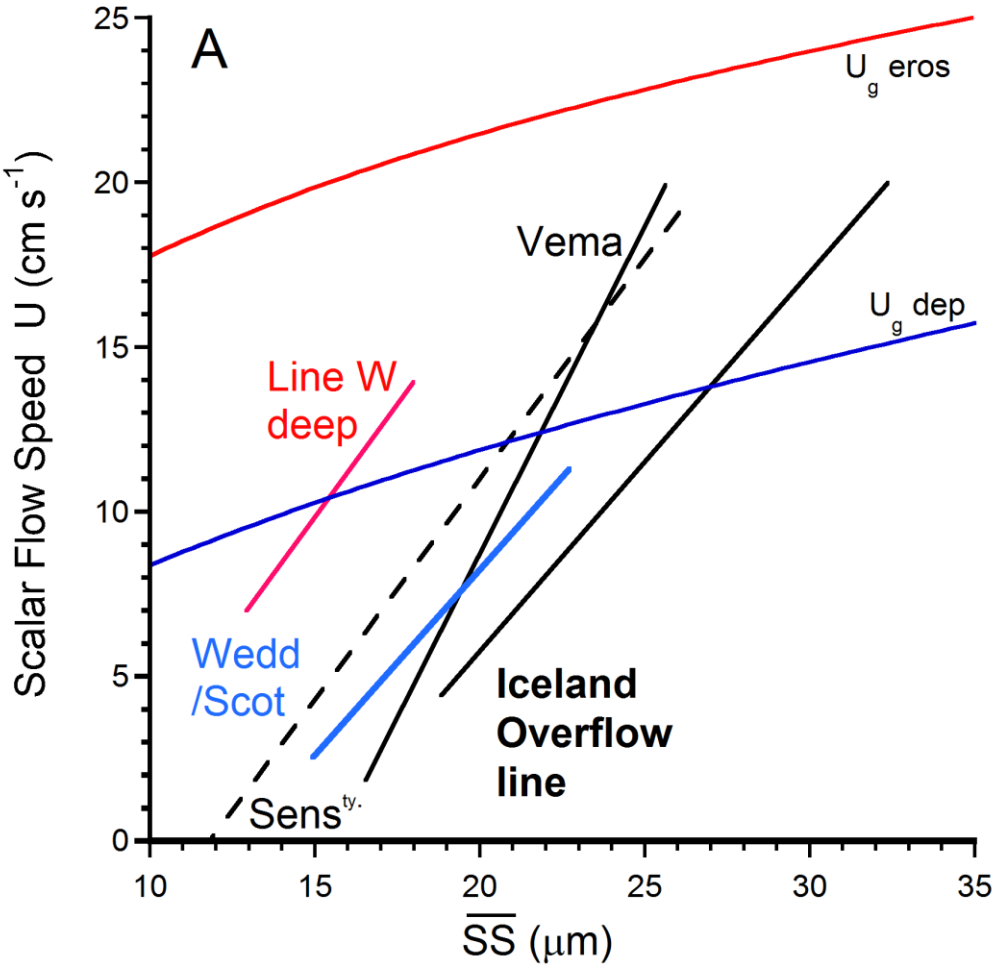

Fig. 7A. *Lines of flow speed vs grain-size plotted as a conventional critical erosion diagram. Lines of flow speed vs grain-size from Fig. 3 and Fig. 1 plotted with the non-cohesive critical deposition condition of Self et al. (1989) and non-cohesive erosion calculated for geostrophic speed. It is clear that the relation of* $\overline{SS}$ *to flow speed is given by neither of the critical conditions. 'Vema' is the rerun Vema Channel line of Fig. 1. The dashed line 'Sens*^{ty}*' is the slope of the sensitivity, arbitrarily located on the U axis.*

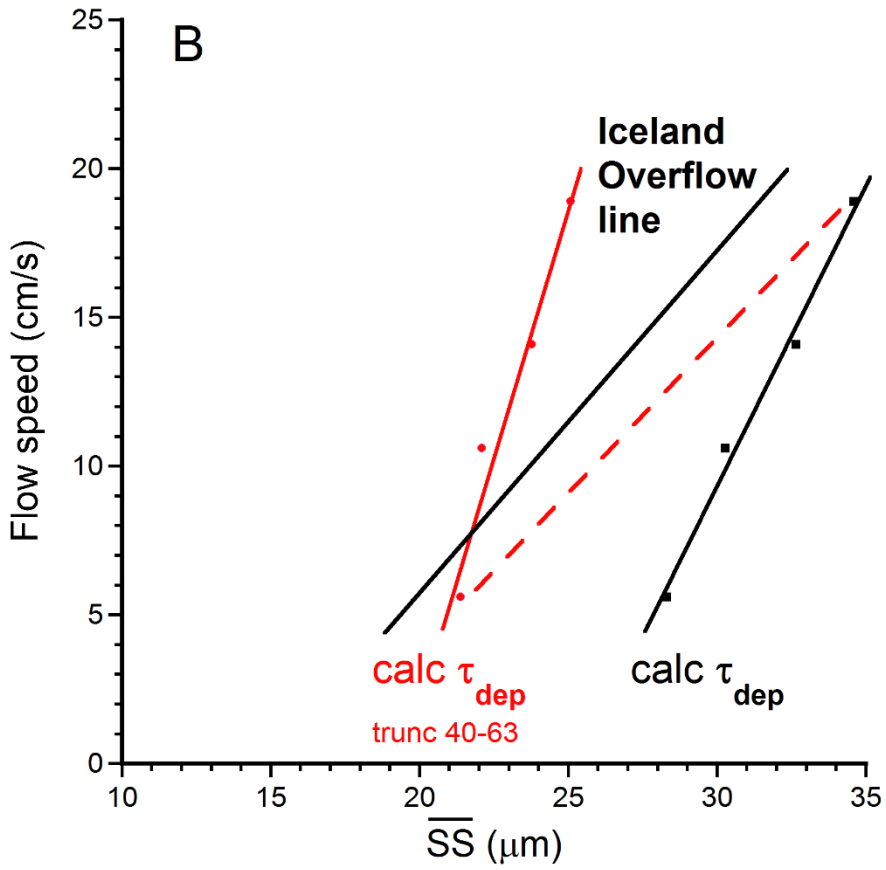

Fig. 7B. *Lines of flow speed vs calculated mean grain-size plotted as a conventional critical erosion diagram. The lines 'calc* τ_{dep}*' are the result of the calculations detailed in section 4.3 for four sets of flow speed data represented by the points. The black line has an input concentration profile* $\propto d^{-2.5}$ *while the red line has that profile truncated by removal of 40-63 μm to simulate 'down-current fining'. Note that the line is shifted to finer sizes, as are Line W deep and Wedd/Scot on Fig. 7A. The red dashed line is what would result from increasing truncation of the 40-63 μm material from none at the fastest speed to complete removal at the slowest.*

4.3 Model of mean size of deposited sediment driven by flow speed data

A simple model to calculate the $\overline{SS}$ mean size of deposited sediment has been implemented which uses the classical Krone equation (Krone, 1962) for the selective deposition of fine suspended material. The amount deposited is given by:

$$\Sigma R_i\, t = \Sigma C_i\, w_{si}\, (1-\tau_o/\tau_{di})\, t$$

where R_i is the rate of deposition (dimensions mass/area.time; $ML^{-2}T^{-1}$), thus $\Sigma R_i\, t$ is (ML^{-2}), to be summed over i = 8 size fractions. Negative values resulting from $\tau_o > \tau_{di}$ are set to zero.

- i = eight logarithmically spaced size fractions from d = 10.0 to d = 63.1 μm, the sortable silt range.
- Settling velocity w_{si} is given by Stokes law $w_{si} = \Delta\rho g d_i^2/18\mu$.
- Critical depositional stress τ_{di} is given by the critical deposition condition of Self et al. (1989) ($\tau_{di} = 0.065\Delta\rho g d_i$) shown on Fig. 7A.
- Deposition is driven by the geostrophic flow speeds U_g with lower limits 0.25, 0.20, 0.15, 0.10 , 0.075 , 0.05, 0.025, 0 m s^{-1} of four representative current meters (# 3,6,7,10 in Table 1) whose data plot on the 'main line' of Fig. 3. The stress τ_o is calculated via a geostrophic drag coefficient $U_g/u_* = 27$ from Bird et al (1982) equivalent to a drag coefficient ($\tau_o./\rho U_g^2$) = 0.0014. [A roughness length z_o = 0.02 cm (Gross et al., 1986) with $U_g = U_{10}$ (speed at 10 mab) in the 'law of the wall' (although well beyond its theoretical validity) gives a very similar value for τ_o.]
- Time t for each flow speed U_g is the proportion of that flow speed range in the current meter record. Therefore if 0.10 to 0.15 m/s occurs for 12% of the record then t = 0.12 for that speed bin and the amount of deposition is $0.12R_i$ for each size fraction.
- The concentration C_i for each fraction is the size distribution of the input from upstream. Here the distribution measured in the most concentrated nepheloid layer by McCave (1983, Sta 13 where C ~ 1 g m^{-3}) has been employed (Supplementary material, item 4). The Coulter Counter data there were presented as cumulative particle number distributions log$N$ = f (log d). In such a distribution a slope of d(log$N$)/d(log$d$) = -3 signifies a flat volume distribution (dV/d(log$d$) = 0) or equal particle volumes in logarithmically increasing size grades (Friedlander, 1977). In the concentrated nepheloid layers McCave (1983) shows slopes in the >10 μm range of ~ -5.5 to -6, equivalent to dV/d(log$d$) = -2.5 to -3. Concentrations in the eight fractions were calculated with the slope = -2.5 from an assumed value of unity in the first (10-12.59 μm) fraction.
- The $\overline{SS}$ size of the deposit is $\Sigma(R_i.t.d_i)$ divided by $\Sigma(R_i.t)$, plotted vs speed in Fig. 7B. The spreadsheet is given as Supplementary Information (Appendix 2.

The rate of deposition for each size fraction is calculated for the range of flow speeds and the deposit resulting from these rates multiplied by the proportion of time in the record that the speed is below a given speed (30, 25, 20 cm s^{-1} etc). The $\overline{SS}$ grain-size of the resulting deposit is then calculated from the amount deposited in each bin times the mid-point diameter divided by the total amount deposited, summed over 8 size bins (10-12.89 ..... 50.1-63.1 μm).

The trend of the resulting line of $\overline{SS}_{calc}$ versus U (Fig. 7B, 'calc τ_{dep}' line based on four current meter records) is fairly similar to that of the various calibration lines and markedly dissimilar to the

critical deposition and erosion curves in Fig. 7A. The whole curve is shifted to coarser sizes than those of the calibration data. By truncating the input size through removal of material 40-63 μm (a simulation of down-current fining) the whole line is shifted to finer sizes (fig. 7B solid red line) albeit with a steeper slope. The red dashed line on Fig. 7B would result from increasing removal of the 40-63 μm material from no removal at the fastest speed to complete removal at the slowest. From this it becomes apparent that the position on the x-axis and slope is also controlled by the input size/concentration distribution. Only close to source is a broad size spectrum supplied. Further down the transport system coarser material is depleted. It would not be appropriate at present to try different concentration-size distributions in an attempt to get a better fit because this is intended simply as a demonstration of the concept rather than a detailed modelling exercise, which remains to be performed. The fact that the slope of the calculated $\overline{SS}$ grain-sizes is similar to the various data sets suggests that the deposit size is controlled by selective deposition in principle as expressed in the Krone equation with suppression of deposition of finer particles at faster flow speeds. This conclusion is similar to that of Mehta and Lott (1989) drawn from their experiments with kaolinite.

4.5 Some implications for existing $\overline{SS}$ records

The derivation of calibrations for the $\overline{SS}$ proxy enables quantification of the flow speed changes implied by records of $\overline{SS}$ in previous studies (see Table, Section 2 in Supplementary Information). These examples also provide an opportunity to test whether the calibration provides feasible values for downcore records from a range of different settings. We focus our attention on published examples from sites that are strongly influenced by deep geostrophic currents, namely the Nordic Overflows, some DWBCs and the ACC. Many of these examples relate to single core site studies, so they cannot constrain any vertical migrations of the main flow axis of the current through time. Hence, future studies that aim to obtain more quantitative estimates of the overall flow speed change and volume flux in a deep sea current, should apply the new $\overline{SS}$ calibration presented here to depth transects of cores. Conversion from flow speeds to volume fluxes will require additional assumptions regarding the cross-sectional area of the geostropic current under investigation (e.g. Thornalley et al 2013a).

A site under the NE Atlantic DWBC south of Iceland (ODP983 60.4˚N, 23.6˚W, 1984 m) demonstrates a tight coupling between changes in flow speed and bottom water properties ($\delta^{18}O$ of *C. wuellerstorfi*) (Fig. 8). The changes are about 10 cm s^{-1} for glacial to interglacial and 4 to 6 cm s^{-1} for stadial to interstadial. A very tight correspondence to benthic $\delta^{18}O$, a water density proxy, with a

slight lead over $\overline{SS}$ suggests density-driven changes in the Iceland-Scotland overflow. With modern flow speeds in the region of ~ 15 cm s^{-1} (Kanzow and Zenk, 2014) the changes can be seen to represent a major change in the source strength of NADW, but not its reduction to zero. Data from a single site have the potential problem of spatial ambiguity because changes in the density structure of the overflow could result in the main axis of the current moving up or down slope. This problem was dealt with by Thornalley et al (2013a and 2013b) who used arrays of cores on the S. Iceland rise and Blake Outer Ridge.

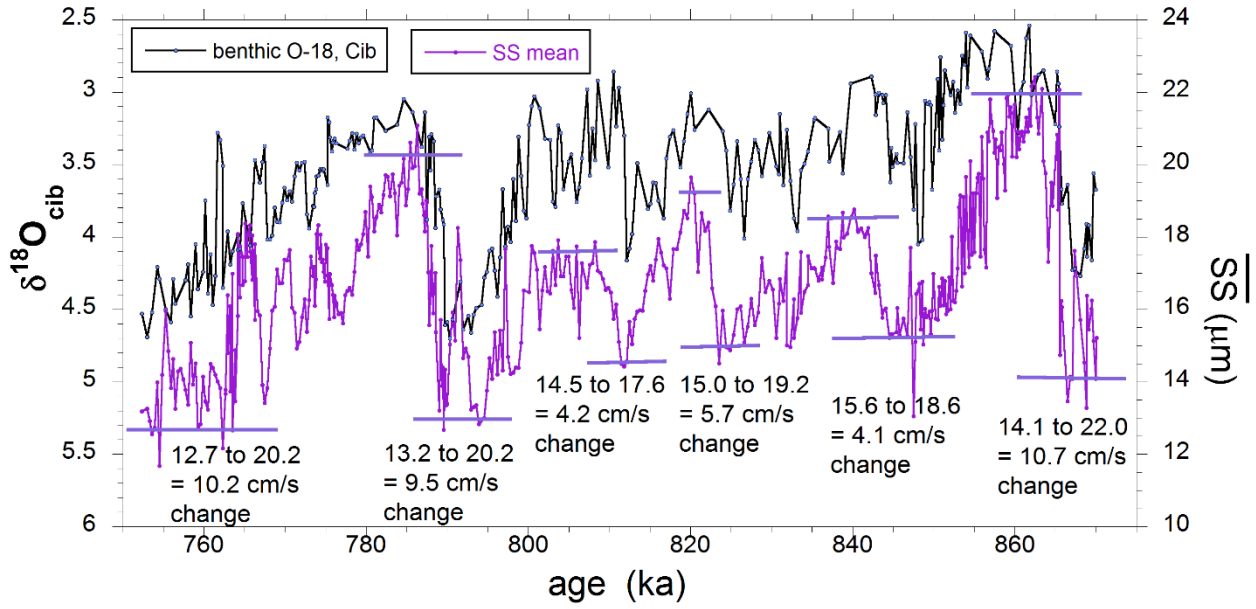

Fig. 8. Benthic $\delta^{18}O$ and $\overline{SS}$ (measured by Sedigraph) on ODP 983 from N. Gardar Drift south of Iceland (Kleiven et al., 2011). The record spans marine isotope stages 22 to 18 containing two major glacial to interglacial transitions with ~10 cm s^{-1} changes and 4-6 cm s^{-1} stadial to interstadial shifts. Modern speeds in the region are ~15 cm s^{-1}.

The magnitude of glacial to inter-glacial (G-IG) changes can now be evaluated at a number of sites around the World (see Table in Supplementary material Section 2). There were complex changes in the North Atlantic DWBC on the Blake Outer Ridge (BOR) with shallow core sites (< 3 km depth) recording faster glacial flow speeds (up to 10 μm coarser, equating to ~14 cm s^{-1}), but more sluggish glacial flow at depths of 3-4 km (3-7 μm finer, equating to ~5-10 cm s^{-1} slower), while the underlying southern source water in the DWBC was ~ 12 -16 cm s^{-1} faster (~9 – 11 μm coarser) during glacials (Yokokawa and Franz, 2002; Thornalley et al., 2013b). The S.W. Pacific DWBC also shows a faster glacial inflow of southern source water, to the Pacific, by 6 cm s^{-1} (4.5 μm , Hall et al., 2001) at a location (Chatham drift) where the present flow is rather slow (2-4 cm s^{-1}, (Warren, 1973; McCave and Carter, 1997), so this represents a very great increase, though, lacking a depth transect, we cannot indicate the volume flux change. There appears to have been little change in the strength of the ACC

in the central Scotia Sea, where G-IG differences basd on 12 cores across the area gave an increase of no more than ~2 cm s^{-1} (McCave et al. 2014). However, Lamy et al. (2015) have shown that changes on the northern margin of Drake Passage, a region not well sampled by McCave et al. (2014), went from weak glacial flow to the modern strong jet under the Sub-Antarctic Front (SAF), a speed change of 16 cm s^{-1}. Overall therefore, the ACC flow through the region increased from G to IG, essentially by the addition of the SAF flow.

The G-IG change in Iceland-Scotland Overflow strength south of Rockall is ~13 cm s^{-1} (McCave et al., 1995b), while on Gardar Drift it is ~11 cm s^{-1} compared with modern speeds of 5 to 19 cm s^{-1} (van Aken and de Boer, 1995; Kleiven et al, 2011), which suggests very slow speeds at the last glacial maximum. Such speeds may not have been sufficient to impart completely a current-sorted signature on the sediment, resulting in an anomaly related to ice-rafted detritus (Jonkers et al., 2015; see Supplementary material section 3C).

The Holocene displays both long-term shifts and shorter term variability. Thornalley et al. (2013a) record a reduction in Iceland-Scotland overflow of some 20%, a mean flow speed change of ~1.8 cm s^{-1}, derived from averaging 13 cores. Farther downstream on Gardar Drift a long-term decline in flow from ~ 9.5 ka to 2 ka of ~8 cm s^{-1} (from 19 μm to 14 μm) is punctuated by major negative excursions around 8.2 and 5 ka (Hoogakker et al, 2011). At this site a current meter at 6.65 mab averages 13 cm s^{-1} (Jonkers et al., 2010), equivalent to a geostrophic speed of 15 cm s^{-1}, thus early Holocene speeds were over 20 cm s^{-1}. This records the major impact on N. Atlantic circulation of the decrease in insolation from the early Holocene maximum. Superimposed on this change are millennial-centennial changes in both Iceland-Scotland and Denmark Strait Overflow strength, some pulsed at 1500 years (Bianchi and McCave, 1999; Ellison et al, 2006; Moffa-Sanchez et al, 2015; Mjell et al, 2015). Many of these changes are of order 5 cm s^{-1}, a large change relative to glacial – interglacial shifts of 10-15 cm s^{-1}, suggesting a Holocene sensitivity of circulation far greater than might be supposed from temperature variations derived from Greenland ice-core records, notwithstanding the potential sensitivity of single core sites to local changes in the positon of the deep-sea current. As higher resolution cores are obtained we are able to estimate the magnitude of change on recent decadal scales associated with climate perturbations such as the NAO and overlapping modern instrumental data. Multi-decadal changes in the flow speed of ISOW in the range of 1 to 2 cm s^{-1} are recorded for the last few hundred years by Boessenkool et al. (2007) and Mjell et al (2016).

5 Conclusions

Correlation of sortable silt mean grain-size, $\overline{SS}$, with the geostrophic flow speed recorded by long-term near-bed current meters has revealed a more complex picture than originally anticipated. Nevertheless, a basis is provided for inference of past flow speed changes and, in favourable circumstances, absolute geostrophic flow speeds. The main points are: (i) Several calibration lines are demonstrated by the correlation of $\overline{SS}$ data from sea bed sediments with flow speeds from nearby long-term current meters. (ii) The slope of the $\overline{SS}$ parameter to flow speed in a normalised plot is relatively constant at 0.74 μm per cm s^{-1} over all the calibration lines. This value allows estimation of *changes* in past flow speeds from $\overline{SS}$ data with the sensitivity of 1.36 ± 0.19 cm s^{-1}/μm for size determined by Sedigraph and 1.47 ± 0.20 cm s^{-1}/μm for size determined by Coulter Counter. Where a site lies close to a probable sediment source, the Iceland overflow region absolute calibration equation $U = 1.31\ \overline{SS} - 17.18$ cm s^{-1} (with $\overline{SS}$ in μm) may be applied. (iii) These data suggest the influence of a deficit of coarse silt (thus finer size for the same speed) at distal sites relative to those sites closer to the sediment source. Moving away from source the availability of coarse silt diminishes due to its depletion by deposition further upstream along the current flow path (progressive down-current fining). This results in a finer $\overline{SS}$ value for a given flow speed. (iv) The trend of the calibration lines is very different from a prediction based on critical deposition or erosion curves. Application of a simple model based on Krone's deposition equation suggests that deposit size is controlled by selective deposition with suppression of deposition of finer particles at faster flow speeds. (v) No effect of eddy (versus mean flow) energy on sediment size is detectable from this data set. (vi) No obvious influence of ice-rafted detritus can be seen in data from the Scotia Sea compared with that from Gardar sediment drift south of Iceland, and reported effects may be due to very slow flows at the LGM unable to sort sediment. As long as the deposit is controlled by currents and accumulation is relatively rapid (>10 cm/ka) the effect of IRD is thus minimal.

Acknowledegments.

We are most grateful for the work of Physical Oceanographers and engineers who have acquired the current meter data used here. Bob Dickson's early compilation of records in WOCE Rept. 46/90 (WCRP 30) to which was added the WOCE database has been particularly important. John Toole helped with the data from line W. The British Oceanographic Data Centre provided some obscure sets and the OSU Buoy Group's compilation of mooring data has been essential. For the sediment samples we thank the Captains and crews of RRS *Charles Darwin* and *James Cook* cruises CD 129, CD159, JC 89 funded by the UK's NERC, RV *Knorr* 198 funded by the Grayce B. Kerr Foundation., RV *Knorr* 197/10 and RV *Endeavor* 539 funded by the NSF (USA). Among the ships of opportunity

thanks to Lloyd Keigwin for RV *Knorr* 197 and 198 who got me to Line W and adjacent sites. In the laboratory Gillian Forman and Simon Crowhurst gave key assistance and Nichole Anest (LDEO repository) and Ellen Roosen (WHOI repository) resampled the original cores of Ledbetter's calibration. Carol Pudsey at BAS provided the Scotia/Weddell Sea data and Rob Pugh did the Scotia Sea Sedigraph work. We are most appreciative of the attention paid to this work by Paul Hill and three anonymous referees. We have also benefitted from discussions with several long-term collaborators (and challengers): Thank you, you know who you are!

References

Andrews, J. T., Principato, S. M., 2002. Grain-size characteristics and provenance of ice-proximal glacial marine sediments. In: Dowdeswell, J. A. and O'Cofaigh, C. (eds), *Geol. Soc. London, Spec. Publ.* **203**, 305-324.

Andrews, J. T., Stein, R., Moros, M., Perner, K., 2016. Late Quaternary changes in sediment composition on the NE Greenland margin (~73° N) with a focus on the fjords and shelf. *Boreas* **45**, 381–397.

Armi, L., D'Asaro, E., 1980. Flow structures of the benthic ocean. *J. Geophys Res.* **85**, 469-484.

Armi, L., Millard, R.C., 1976. The bottom boundary layer of the deep ocean. *J. Geophys Res.* **81**, 4983-4990.

Amos, C.L., Daborn, G.R., Christian, H.A., Atkinson, A., Robertson, A., 1992. *In situ* erosion measurements on fine-grained sediments from the Bay of Fundy. *Mar. Geol.* **108**, 175–196.

Bianchi, G.G., McCave, I.N., 1999. Holocene periodicity in North Atlantic climate and deep-ocean flow south of Iceland. *Nature* **397**, 515-517

Bianchi, G.G., McCave, I.N., 2000. Hydrography and sedimentation under the deep western boundary current on Björn and Gardar Drifts, Iceland Basin. *Mar. Geol.* **165**, 137–169.

Bianchi, G.G., Hall, I.R., McCave, I.N., Joseph, L., 1999. Measurement of the sortable silt current speed proxy using the Sedigraph 5100 and Coulter Multisizer IIe: Precision and accuracy. *Sedimentology* **46**, 1001-1014.

Bird, A.A., Weatherly G.L., Wimbush M., 1982. A study of the bottom boundary-layer over the Eastward scarp of the Bermuda Rise. *J. Geophys Res.* **87**, 7941-7954.

Boessenkool, K. P., Hall, I. R., Elderfield, H., Yashayaev, I., 2007. North Atlantic climate and deep-ocean flow speed changes during the last 230 years, *Geophys. Res. Lett*. **34**, L13614, doi:10.1029/2007gl030285

Coakley, J.P. and Syvitski, J.P.M., 1991. SediGraph technoque. In Syvitski, J.P.M. (Ed.) *Principles, methods, and application of particle size analysis*. Cambridge Univ. Press, p. 129-142.

Csanady, G.T., 1972. Geostrophic drag, heat and mass transfer coefficients for the diabatic Ekman layer. *J. Atmos. Sci*. **29**, 488-496.

Curry, W.B. and D. W. Oppo, D.W., 2005. Glacial water mass geometry and the distribution of $\delta^{13}C$ of ΣCO_2 in the western Atlantic Ocean, Paleoceanography, **20**, Art. No. PA1017, 12 pp

Dade, W. B., Nowell, A. R. M., Jumars, P. A., 1992. Predicting erosion resistance of muds, *Mar. Geol*. **105**, 285-297.

Dickson, R.R., 1983. Global summaries and intercomparisons: Flow statistics from long-term current meter moorings. In: Robinson, A.R. (Ed.), *Eddies in Marine Science*, Springer-Verlag, Berlin, pp. 278-353

Drake, D.E., Cacchione, D.A., 1986. Field observations of bed shear-stress and sediment resuspension on continental shelves, Alaska and California. *Continental Shelf Res.* **6**, 415-429.

Driscoll, M.L., Tucholke, B.E., McCave, I.N., 1985. Seafloor zonation in sediment texture on the Nova Scotian lower continental rise. *Mar. Geol.* **66**, 25-41.

Dyer, K.R., 1986. *Coastal and estuarine sediment dynamics*. J. Wiley, Chichester, UK, 342 pp.

Einstein, H. A., Krone, R.B., 1962. Experiments to determine modes of cohesive sediment transport in salt water, *J. Geophys Res.* **67**, 1451-1461.

Eittreim S.L., Ewing, M., Thorndike, E.M., 1969. Suspended matter along the continental margin of the North American Basin. *Deep Sea Res*. **16**, 613-624.

Ellison, C.R.W., Chapman, M.R., Hall, I.R., 2006. Surface and deep ocean interactions during the cold climate event 8200 years ago. *Science* **312**, 1929-1932.

Friedlander, S.K., 1977. Smoke, dust and haze: Fundamentals of aerosol behaviour. Wiley, New York, 317 pp.

Gardner, W.D., Sullivan, L.G., 1981. Benthic storms: temporal variability in a deep-ocean nepheloid layer, *Science* **213**, 329-331.

Gross, T. F., Williams, A.J., 1991. Characterization of deep-sea storms, *Mar. Geol.* **99**, 281-301.

Gross, T.F., Williams, A.J., Grant, W.D., 1986. Long-term in situ calculations of kinetic energy and Reynolds stress in a deep sea boundary layer. *J. Geophys. Res.* **91**, 8461-8469.

Hall, I.R., McCave, I.N., Shackleton, N.J., Weedon, G.P., Harris, S.E., 2001. Intensified deep Pacific inflow and ventilation during Pleistocene glacial times. *Nature* **412**, 809-812.

Hamm, N.T., Dade, W. B., 2013. A laboratory study of dynamic sorting of fine, non-cohesive particles by steady, unidirectional currents. *Mar. Geol.* **336**, 215-222.

Haskell, B. J., Johnson, T. C., 1993, Surface sediment response to deep-water circulation on the Blake Outer Ridge, Western North Atlantic – Paleoceanographic implications, *Sediment. Geol*. **82**, 133–144.

Hjulstrom, F., 1939. Transportation of detritus by moving water. In: Trask, P. D. (Ed.), *Recent Marine Sediments*. Am. Assoc. Petroleum Geologists, Tulsa, pp. 5-31.

Hollister, C. D., Heezen, B.C., 1972. Geologic effects of ocean bottom currents: western North Atlantic, In: Gordon , A.L. (Ed.), *Studies in Physical Oceanography, Vol. II*, Gordon Breach, New York, pp. 37-66.

Hollister, C.D., McCave, I.N., 1984. Sedimentation under deep-sea storms. *Nature* **309**, 220-225.

Hoogakker, B., Chapman, M.R., McCave, I.N., Hillaire-Marcel, C., Ellison, C., Hall, I.R. and Telford, I., 2011. Dynamics of North Atlantic deep water masses during the Holocene. *Paleoceanography* **26**, PA4214, 10 pp., doi:10.1029/2011PA002155

Jessen, S.P., Rasmussen, T.L., 2015. Sortable silt cycles in Svalbard slope sediments 74–0 ka. *J. Quat. Sci.* **30**, 743–753.

Jonkers, L., Mienis, F., Boer, W., Hall, I.R., Brummer, G.-J.A., 2010. Intra-annual variability of extremely rapid sedimentation onto Gardar Drift in the northern North Atlantic. *Deep-Sea Research I* **57**, 1027–1038.

Jonkers, L., Barker, S., Hall, I. R., Prins, M. A., 2015. Correcting for the influence of ice-rafted detritus on grain-size-based paleocurrent speed estimates. *Paleoceanography*, **30**, 1347–1357. doi:10.1002/2015PA002830.

Kanzow, T and Zenk, W., 2014. Structure and transport of the Iceland Scotland Overflow plume along the Reykjanes Ridge in the Iceland Basin. *Deep-Sea Research I* **86**, 82–93.

Kleiven, H.F., Hall, I.R., McCave, I.N., Knorr, G., Jansen, E., 2011. Coupled deep-water flow and climate variability in the Mid-Pleistocene North Atlantic. *Geology* **39**, 343-346.

Krone, R.B., 1962. *Flume studies of the transport of sediment in estuarial shoaling processes.* Final Report to Corps of Engineers, Hydraulic Engineering Laboratory and Sanitary Engineering Research Laboratory, University of California, Berkeley, 110 pp.

Krumbein, W.C., 1938. Size frequency distribution of sediments and the normal phi curve. *J. Sediment. Petrol.* **8**, 84-90.

Lamy, F., Arz, H.W., Kilian, R., Lange, C.B., Lembke-Jene, L., Wengler, M., Kaiser, J., Baeza-Urrea, O., Hall, I.R., Harada, N., Tiedemann, R., 2015. Glacial reduction and millennial-scale variations in Drake Passage throughflow. *Proc. Natl. Acad. Sci. U.S.A.* **112**, 13496–13501. doi:10.1073/pnas.1509203112

Law, B. A., Hill, P. S., Milligan, T. G., Curran, K. J., Wiberg, P. L., Wheatcroft, R. A.,2008. Size sorting of fine-grained sediments during erosion: Results from western Gulf of Lions. *Continental Shelf Res.* **28**, 1935–1946

Ledbetter, M.T., 1986. A late Pleistocene time-series of bottom-current speed in the Vema Channel. *Palaeogeog., Palaeoclimatol., Palaeoecol.* **53**, 97-105.

Ledbetter M.T., Johnson D.A., 1976. Increased transport of Antarctic Bottom Water in Vema Channel during last Ice Age. *Science* **194**, 837-839.

Li, G., Piper, D.J.W., 2015. The influence of meltwater on the Labrador Current in Heinrich Event 1 and the Younger Dryas. *Quat. Sci. Rev.* **107**, 129-137

Mantz, P.A. 1977. Incipient transport of fine grains and flakes by fluids - extended Shields diagram. *J. Hydraul. Div.-ASCE* **103**, 601-615

McCave, I.N., 1983. Particulate size spectra, behaviour and origin of nepheloid layers over the Nova Scotian Continental Rise. *J. Geophys Res.* **88**, 7647-7666.

McCave, I.N., 1985. Stratigraphy and sedimentology of box cores from the HEBBLE site on the Nova Scotian Continental Rise. *Mar. Geol.* **66**, 59-89.

McCave, I.N. 2008a, Size sorting during transport and deposition of fine sediments: Sortable silt and flow speed. In: Rebesco, M., Camerlenghi, A. (Eds.), *Contourites*, Elsevier, Amsterdam, pp. 121-142.

McCave, I.N., 2008b. Nepheloid layers. In: J.H. Steele, et al. (Eds), *Encyclopedia of Ocean Sciences*, Academic Press, Oxford, 2nd edition, online**,** http://dx.doi.org/10.1016/B978-012374473-9.00671-8, p. 4086-4096. (2009, 2nd edition, print, vol. **4**, pp 8-18)

McCave, I.N., Carter, L., 1997. Recent sedimentation beneath the deep western boundary current off northern New Zealand. *Deep-Sea Res.* **44,** 1203-1237.

McCave I.N., Hall, I.R., 2006. Size sorting in marine muds: Processes, pitfalls and prospects for palaeoflow-speed proxies. *Geochem. Geophys. Geosyst*. **7**, Q10N05, 37 pp. doi: 10.1029/2006GC001284.

McCave, I.N., Lonsdale, P.F., Hollister, C.D., Gardner, W.D., 1980. Sediment transport over the Hatton and Gardar contourite drifts. *J. Sediment. Petrol*. **50**, 1049-1062.

McCave, I.N., Manighetti, B., Robinson, S.G., 1995a. Sortable silt and fine sediment size/ composition slicing: parameters for palaeocurrent speed and palaeoceanography. *Paleoceanography* **10**, 593-610.

McCave, I. N., Manighetti, B., Beveridge, N. A. S., 1995b. Circulation in the glacial North Atlantic inferred from grain-size measurements, *Nature*, **374**, 149–152.

McCave I.N., Swift, S.A. 1976. A physical model for the rate of deposition of fine-grained sediment in the deep sea. *Geol. Soc. America Bull.* **87**, 541-546.

McCave, I.N., Crowhurst, S.C., Kuhn, G., Hillenbrand, C.-D., Meredith, M.P., 2014. Minimal change in Antarctic Circumpolar Current flow speed between the last Glacial and Holocene. *Nature Geoscience*, **7**, 113-116. doi:10.1038/ngeo2037.

McManus, J. F., Francois, R., Gherardi, J.-M., Keigwin, L.D. and Brown-Leger, S., 2004), Collapse and rapid resumption of Atlantic meridional circulation linked to deglacial climate changes, *Nature*, 428, 834-837.

Mehta, A. J., Letter, J.V., 2013, Comments on the transition between cohesive and cohesionless sediment bed exchange, *Estuarine, Coastal and Shelf Sci.* **131**, 319-324.

Mehta A.J., Lott, J.W. 1987. Sorting of fine sediment during deposition. In: Kraus, N.C. (Ed.), *Coastal Sediments '87*, American Society of Civil Engineers, New York, pp. 348-362.

Migniot, C., 1968. Étude des propriétés physiques de différents sediments trés fins et de leur comportement sous des actions hydrodynamiques. *Houille Blanche* **7**, 591-620.

Miller, M.C. and Komar, P.D. 1977. The development of sediment threshold curves for unusual environments (Mars) and for inadequately studied materials (foram sands). *Sedimentology* **24**, 709-721

Miller, M.C., McCave, I.N., Komar, P.D., 1977. Threshold of sediment motion under unidirectional currents. *Sedimentology* **24**, 507-527.

Miller, R.L., Kahn, J.S. 1962. *Statistical Analysis in the Geological Sciences*, J. Wiley, New York, 483 p.

Milligan,T.G. and Kranck, K., 1991. Electroresistance particle size counters, In Syvitski, J.P.M. (Ed.) *Principles, methods, and application of particle size analysis*. Cambridge Univ. Press, p. 109-118.

Mitchener H., Torfs, H., 1996. Erosion of mud/sand mixtures. *Coastal Engineering* **29**, 1-25.

Mjell, T.L., Ninnemann, U.S., Eldevik, T., Kleiven H.(K.) F., 2015, Holocene multidecadal- to millennial-scale variations in Iceland-Scotland overflow and their relationship to climate, *Paleoceanography* **30**, doi:10.1002/ 2014PA002737

Mjell, T. L., Ninnemann, U. S. Kleiven, H. F., Hall I. R., 2016. Multidecadal changes in Iceland Scotland Overflow Water vigor over the last 600 years and its relationship to climate, *Geophys. Res. Lett.*, **43**, doi:10.1002/2016GL068227.

Moffa-Sanchez, P., Hall I.R., Thornalley D.J.R., Barker S., Stewart, C., 2015. Changes in the strength of the Nordic Seas Overflows over the past 3000 years. *Quat. Sci. Rev.* **123**, 134-143.

Niño, Y., Lopez, F., Garcia, M., 2003. Threshold for particle entrainment into suspension. *Sedimentology* **50**, 247-263.

Pettijohn, F.J., 1975. *Sedimentary Rocks.* 3rd Ed., Harper and Row, New York, 628 pp.

Piotrowski, A.M., Goldstein, S.L., Hemming, S.R. and R. G. Fairbanks, R.G., 2004. Intensification and variability of ocean thermohaline circulation through the last deglaciation, *Earth Planet. Sci. Lett.* 225, 205-220.

Pugh, R.S., 2007. *Late Quaternary Changes in the Antarctic Circumpolar Current in the Scotia Sea*. Ph.D. thesis University of Cambridge, 192 pp.

Rebesco, M., Camerlenghi, A., (Eds), 2008. *Contourites*. Elsevier, Amsterdam, 663 pp.

Self, R.F.L., Nowell, A.R.M., Jumars, P.A., 1989. Factors controlling critical shears for deposition and erosion of individual grains. *Mar. Geol.* **86**, 181-199.

Smalley, I.J., 1966. Origin of quartz sand. *Nature* **211**, 476-479.

Sorby, H.C., 1859. On the structures produced by the currents present during the deposition of stratified rocks. *The Geologist*, **2**, 137-146.

Spinrad, R.W., Zaneveld, J.R.V., 1982 An analysis of the optical-features of the near-bottom and bottom nepheloid layers in the area of the Scotian rise. *J. Geophys. Res.* **87**, 9553-9561.

Talling, P.J., Paull, C.K., Piper, D.J.W., 2013. How are subaqueous sediment density flows triggered, what is their internal structure and how does it evolve? Direct observations from monitoring of active flows. *Earth-Sci. Rev.* **125**, 244–287.

Teeter, A.M.., Parchure, T.M. McAnally, W.H., 1997. Size-dependant erosion of two silty-clay sediment mixtures. In: Burt, N., et al. (Eds.) *Cohesive Sediments*, J. Wiley, Chichester, UK, pp. 253-262.

Thornalley, D.J.R., Blaschek, M., Davies, F.J., Praetorius, S., Oppo, D.W. , McManus, J.F., Hall, I.R., Kleiven, H., Renssen, H., McCave. I.N., 2013a, Long-term variations in Iceland-Scotland overflow strength during the Holocene. *Climate of the Past* **9**, 2073–2084.

Thornalley, D. J. R., Barker, S., Becker, J., Hall, I.R., Knorr, G., 2013b, Abrupt changes in deep Atlantic circulation during the transition to full glacial conditions, *Paleoceanography* **28**, 253–262. doi:10.1002/palo.20025.

van Aken, H.M., de Boer, C.J., 1995. On the synoptic hydrography of intermediate and deep water masses in the Iceland Basin. *Deep-Sea Res.* **21**, 165-189.

Warren, B. A., 1973. Transpacific hydrographic sections at latitudes 43°S and 28°S; the SCORPIO Expedition - II. Deep water. *Deep-Sea Res.* **20**, 9-38.

Warren, B.A., 1981. Deep circulation of the world ocean, In Warren, B.A. and Wunsch C., (Eds),, *Evolution of Physical Oceanography*, MIT Press, Cambridge, Mass., 6-41.

Warren, B.A., Whitworth, T., LaCasce, J.H., 2002. Forced resonant undulation in the deep Mascarene Basin. *Deep-Sea Res. Part II* **49**, 1513-1526.

Weaver, P. P. E., Thomson, J., 1993. Calculating erosion by deep-sea turbidity currents during initiation and flow. *Nature* **364**, 136–138.

Wheatcroft, R.A., Butman, C.A., 1997. Spatial and temporal variability in aggregated grain-size distributions, with implications for sediment dynamics. *Continental Shelf Res.* **17**, 367-390.

White, S.J. 1970. Plane bed thresholds of fine grained sediments. *Nature* **228**, 152-154.

Winterwerp, J.C., van Kesteren, W. G. M., van Prooijen, B., Jacobs, W., 2012. A conceptual framework for shear flow–induced erosion of soft cohesive sediment beds. *J. Geophys Res.* **117**, C10020, doi:10.1029/2012JC008072.

Yokokawa, M., Franz, S.O., 2002. Changes in grain-size and magnetic fabric at Blake–Bahama Outer Ridge during the late Pleistocene (Marine Isotope Stages 8–10). *Mar. Geol.* **189**, 123–144.

Table Captions

Table 1. Sediment sample and current meter locations and data

Table 2. Slope data for lines fitted to $\overline{SS}$ and U data by RMA

Appendix A. Supplementary material for McCave, Thornalley and Hall,

"*Relation of sortable silt grain size to deep-sea current speeds: Calibration of the 'Mud Current Meter'* "

1. **Maps of sampled sites.**

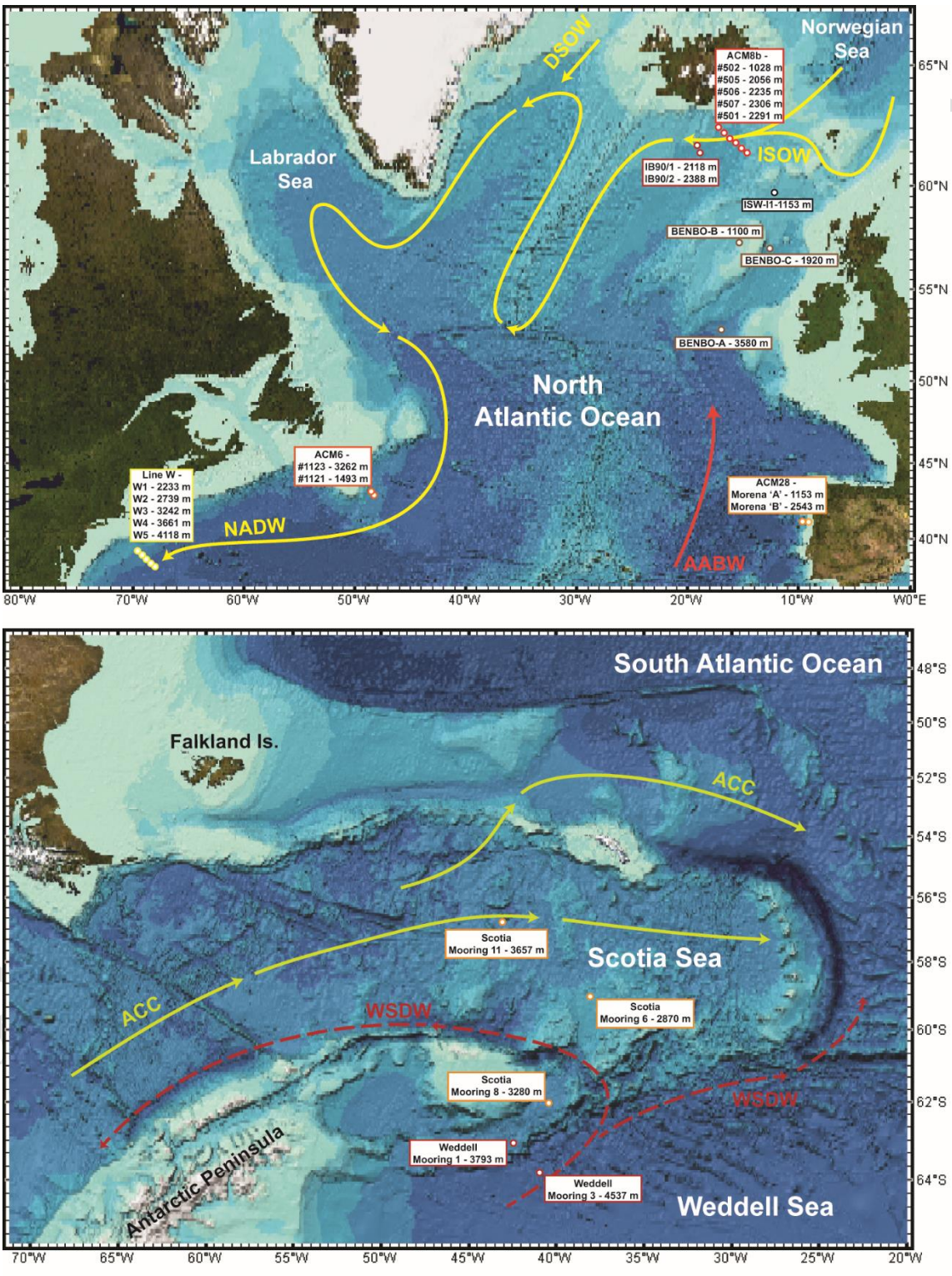

2. Table. Ranges of $\overline{SS}$ for published records

	instru-ment	Inter-glacial	glacial	range µm	speed change	Ref # in Supp. Info.
Glacial-Interglacial Records						
S Feni Drift	Sedi	28	18.5	9.5	12.9	11
N.Gardar Drift	Sedi	22	14	8	10.9	9
Iberian margin	Sedi	21	14.5	6.5	8.8	6
CGFZ	Sedi	21	10.5	10.5	14.3	5
Bermuda rise	Sedi	20	10.5	9.5	12.9	5
BOR (GNAIW)	CC	22	32	-10	-14.7	17
BOR(NADW)	CC	21.5	18	3.5	5.1	17
BOR (AABW)	CC	18	29	-11	-16.2	17
BOR (NADW)	Sedi	23	16	7	9.5	18
BOR (AABW)	Sedi	14	23	-9	-12.2	18
Ceara Rise	Sedi	17.8	15	2.8	3.8	4
Chatham	Sedi	13.5	18	-4.5	-6.1	7
ACC Central Scotia	CC	17.5	16.25	1.25	1.8	12
ACC Drake Passage	Sedi	36	24	12	16.3	10
Holocene Records		Holo max	Holo min	range	speed change	
S. Iceland	Sedi			-1.3	-1.8	16
S. Iceland	CC	17.9	20.6	-2.7	-4.0	13
central Gardar Drift	Sedi	15.5	11.5	4	5.4	1
central Gardar Drift	CC	14.5	19.5	-5	-7.4	8
central Gardar Drift	CC	19.3	16	3.3	4.9	3
S. Iceland	CC	30.5	34.5	-4	-5.9	15
Eirik Drift	CC	24.5	21	3.5	5.1	15
S. Iceland	CC	17.8	19.1	-1.3	-1.9	14
central Gardar Drift	CC	16.1	15.4	0.7	1.0	2

Negative is slowdown (from older to younger)

Conversion of Sedigraph to laser values, specific to the laser sizer in use, will be required if the calibration presented in this study is to be applied to laser data. Jessen and Rasmussen (2015) have comparative data for the LS230 laser and Sedigraph (but no equation) while Jonkers et al. (2015) compare Fritsch and Coulter counter. For Jonkers' data $\overline{SS}_{(CC)} = 1.001*\overline{SS}_{(laser)} - 0.74$ ($r^2 = 0.442$).

References for Table.

1. Bianchi, G.G., McCave, I.N., 1999. Holocene periodicity in North Atlantic climate and deep-ocean flow south of Iceland. *Nature* **397**, 515-517.
2. Boessenkool, K. P., Hall, I. R., Elderfield, H., Yashayaev, I., 2007. North Atlantic climate and deep-ocean flow speed changes during the last 230 years, *Geophys. Res. Lett*. **34**, L13614. doi:10.1029/2007gl030285

3. Ellison, C.R.W., Chapman, M.R., Hall, I.R., 2006. Surface and deep ocean interactions during the cold climate event 8200 years ago. *Science* **312**, 1929-1932.
4. Gröger, M., R. Henrich, T. Bickert, 2003. Glacial-interglacial variability in lower North Atlantic Deep Water: Inference from silt grain size analysis and carbonate preservation in the western equatorial Atlantic, *Mar. Geol*. **201**, 321–332.
5. Hall, I. R., I. N. McCave, M. R. Chapman, and N. J. Shackleton (1998), Coherent deep flow variation in the Iceland and American basins during the last interglacial, *Earth Planet. Sci. Lett.* **164**, 15–21.
6. Hall, I.R. and McCave, I.N. 2000. Palaeocurrent reconstruction, sediment and thorium focussing on the Iberian margin over the last 140 ka. *Earth Planet. Sci. Lett.* **178**, 151-164.
7. Hall, I. R., I. N. McCave, N. J. Shackleton, G. P. Weedon, and S. E. Harris, 2001. Intensified deep Pacific inflow and ventilation in Pleistocene glacial times, *Nature* **412**, 809–812.
8. Hoogakker, B., Chapman, M.R., McCave, I.N., Hillaire-Marcel, C., Ellison, C., Hall, I.R. and Telford, I., 2011. Dynamics of North Atlantic deep water masses during the Holocene. *Paleoceanography* **26**, PA4214, 10 pp. doi:10.1029/2011PA002155
9. Kleiven, H.F., Hall, I.R., McCave, I.N., Knorr, G., and Jansen, E., 2011. Deep-water formation and climate change in the North Atlantic during the Mid-Pleistocene. *Geology* **39**, 343–346.
10. Lamy, F., Arz, H.W., Kilian, R., Lange, C.B., Lembke-Jene, L., Wengler, M., Kaiser, J., Baeza-Urrea, O., Hall, I.R., Harada, N., Tiedemann, R., 2015. Glacial reduction and millennial-scale variations in Drake Passage throughflow. *Proc. Natl. Acad. Sci. U.S.A.* **112**, 13496–13501. doi:10.1073/pnas.1509203112
11. McCave, I. N., B. Manighetti, and N. A. S. Beveridge 1995. Circulation in the glacial North Atlantic inferred from grain size measurements, *Nature* **374**, 149–152.
12. McCave, I.N., Crowhurst, S.C., Kuhn, G., Hillenbrand, C.-D. and Meredith, M.P. 2014. Minimal change in Antarctic Circumpolar Current flow speed between the last Glacial and Holocene. *Nature Geoscience*, **7**, 113-116. doi:10.1038/ngeo2037.
13. Mjell, T. L., Ninnemann, U. S., Eldevik, T., Kleiven H. (K.) F., 2015. Holocene multidecadal- to millennial-scale variations in Iceland-Scotland overflow and their relationship to climate, *Paleoceanography* **30**, doi:10.1002/ 2014PA002737.
14. Mjell, T. L., Ninnemann, U. S. Kleiven, H. F., Hall I. R., 2016. Multidecadal changes in Iceland Scotland Overflow Water vigor over the last 600 years and its relationship to climate, *Geophys. Res. Lett.* **43**, doi:10.1002/2016GL068227.
15. Moffa-Sanchez, P., Hall, I.R.; Thornalley, D.J. R., Barker, S., 2015. Changes in the strength of the Nordic Seas overflows over the past 3000 years. *Quat. Sci. Rev.* **123**, 134-143.
16. Thornalley, D.J.R., Blaschek, M., Davies, F.J., Praetorius, S., Oppo, D.W., McManus, J.F., Hall, I.R., Kleiven, H., Renssen, H., McCave, I.N., 2013a. Long-term variations in Iceland-Scotland overflow strength during the Holocene. *Clim. Past* **9**, 2073-2084. doi: 10.5194/cp-9-2073-2013.
17. Thornalley, D. J. R., Barker, S., Becker, J., Hall, I.R., Knorr, G., 2013b. Abrupt changes in deep Atlantic circulation during the transition to full glacial conditions, *Paleoceanography* **28**, 253–262. doi:10.1002/palo.20025.
18. Yokokawa, M., Franz, S.O., 2002. Changes in grain size and magnetic fabric at Blake–Bahama Outer Ridge during the late Pleistocene (Marine Isotope Stages 8–10). *Mar. Geol.* **189**, 123–44.

3. $\overline{SS}$ vs SS% data by laser sizer

Examples of current-sorted sediment from areas of IRD input.

A. Data from Marshall et al (2014)

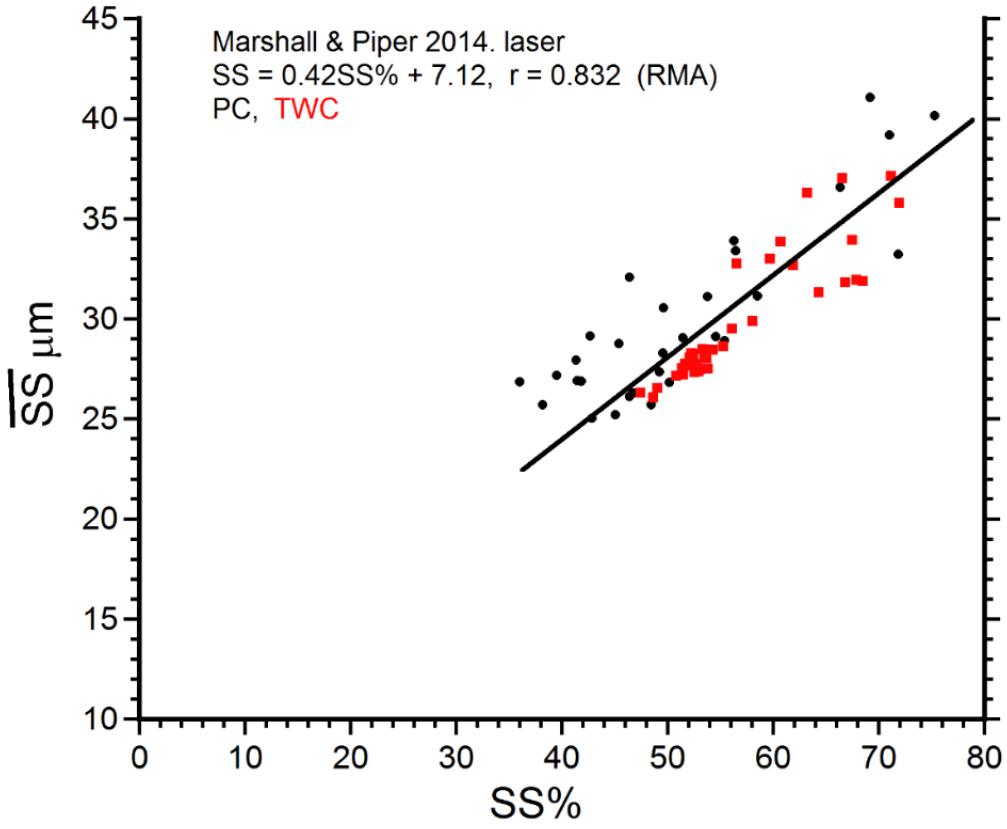

PC = Piston core; TWC = Trigger weight core.

B. $\overline{SS}$ vs SS% from Li and Piper (2015) by laser sizer.

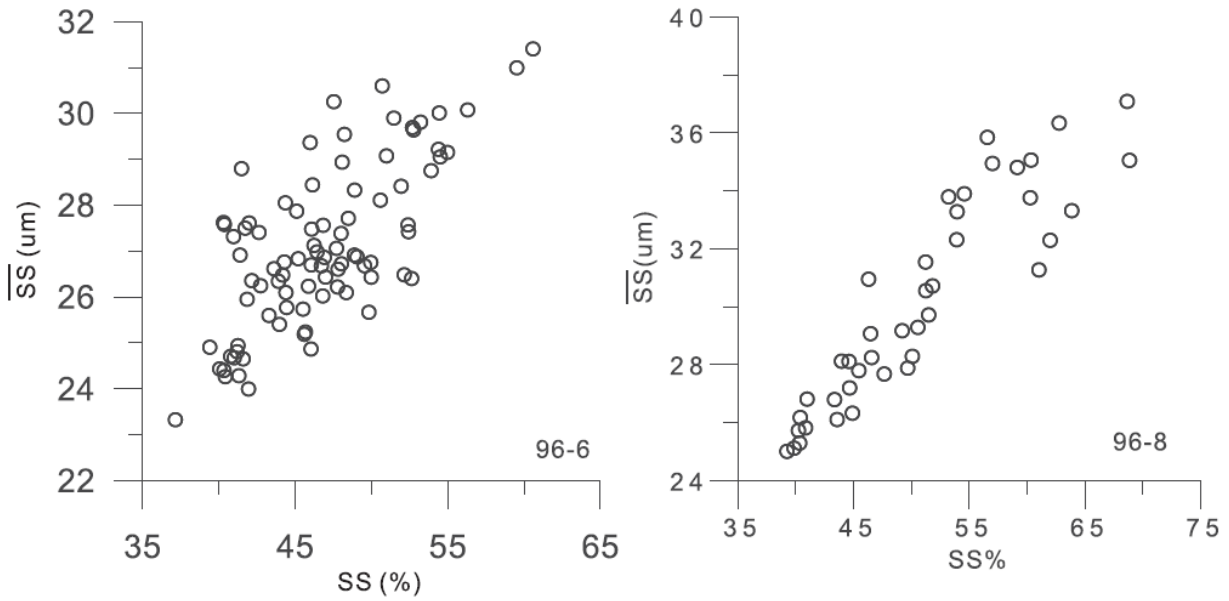

C. Example of poorly sorted sediment where an IRD signature probably dominates the $\overline{SS}$ calculated from Jonkers et al. (2015) laser sizer data. Compared with the plots above in a) and b) there is a great deal of scatter signifying the presence of unsorted material and supporting the inference of Jonkers et al. that this data set contains data from sediments that have not responded to current-sorting. We argue that this was caused by very slow flow speeds at the LGM.

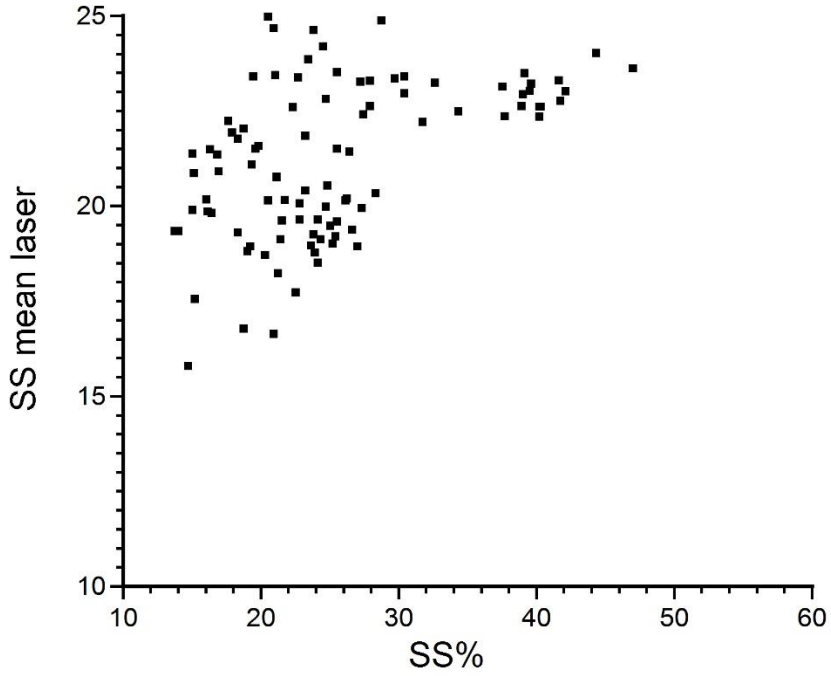

4. Size distributions in nepheloid layer from McCave (1983)

Cumulative particle number distributions, log-log plot. Abscissa has size-doubling increments with each curve (#s 10 to 01) starting one position to the right successively. Maximum slopes are -5.5 to -6, equivalent to volume distributiond with slopes -2.5 to -3. A cumulative number slope of -3 (a Junge distribution) is equivalent to a flat volume distribution, slope = 0 (McCave 1983, 1984).

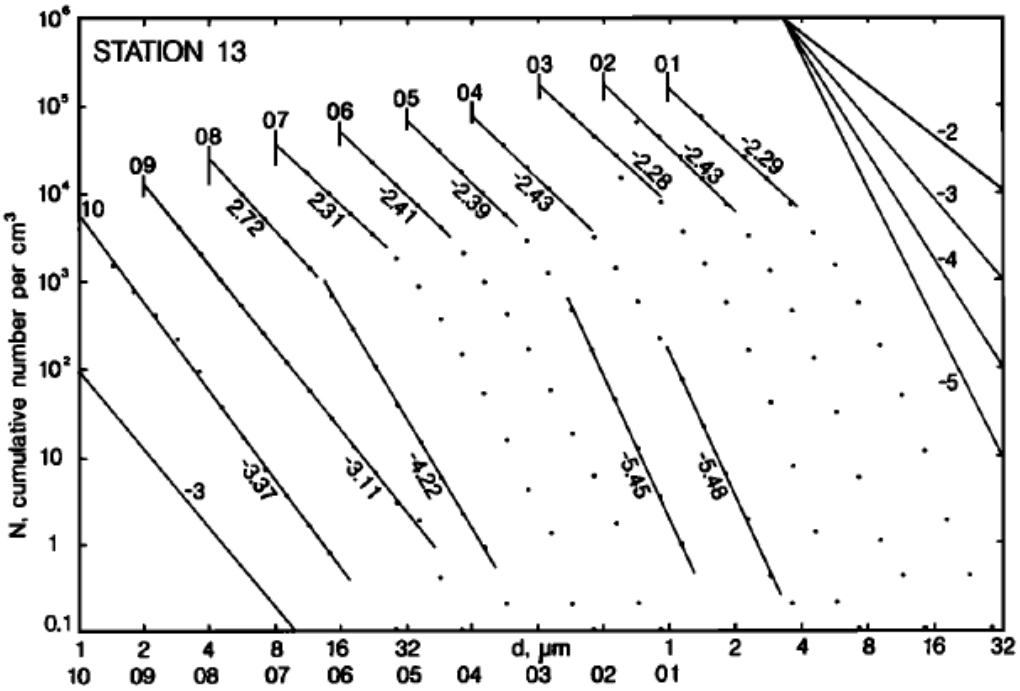

5. Data on grain-size distributions of proximal glacial marine sediments from the Ross Sea and E. Greenland shelf from Andrews and Principato (2003)

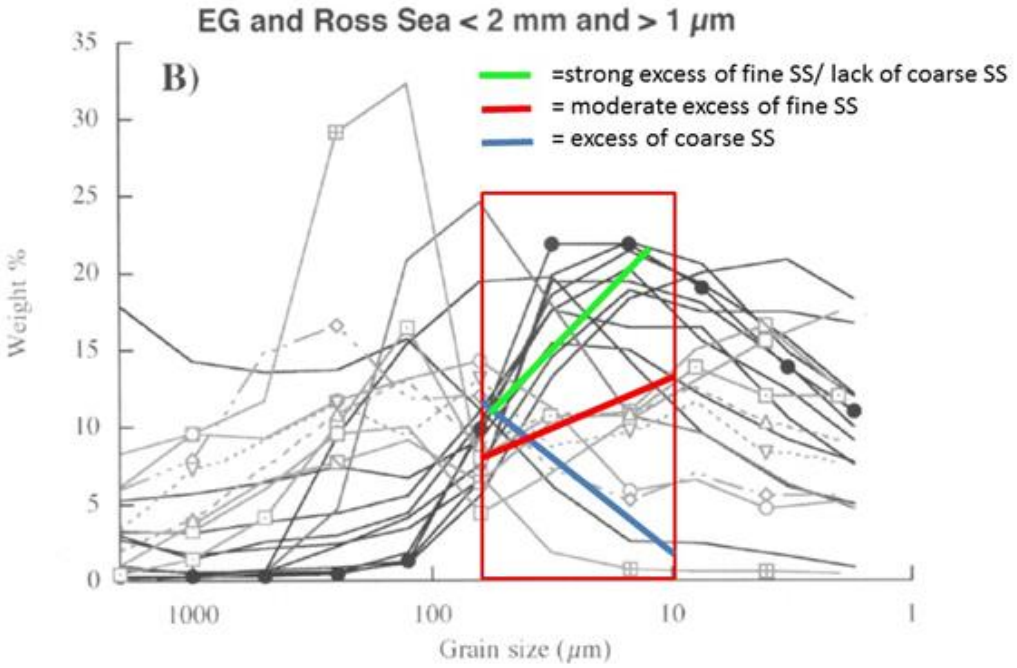

The red box delineates the SS size range. Light grey is Ross Sea, black is E. Greenland data

References

Andrews, J.T., Principato S. M. 2002. Grain-size characteristics and provenance of ice-proximal glacial marine sediments. In: Dowdeswell, J. A. and O'Cofaigh, C. (eds), *Geol. Soc. London, Spec. Publ.* **203**, 305-324.

Jonkers, L., Barker, S., Hall, I. R., Prins, M. A., 2015. Correcting for the influence of ice-rafted detritus on grain-size-based paleocurrent speed estimates. *Paleoceanography* **30**, 1347–57.

Li, G., Piper, D.J.W., 2015. The influence of meltwater on the Labrador Current in Heinrich event 1 and the Younger Dryas. *Quat. Sci. Rev.* **107**, 129-137.

Marshall, N.R., Piper, D.J.W., Saint-Ange, F., Campbell, D.C., 2014, Late Quaternary history of contourite drifts and variations in Labrador Current flow, Flemish Pass, offshore eastern Canada. *Geo-Mar Lett*. **34**, 457–470. doi 10.1007/s00367-014-0377-z

McCave, I.N., 1983. Particulate size spectra, behaviour and origin of nepheloid layers over the Nova Scotian Continental Rise. *J. Geophys Res.* **88**, 7647-7666.

McCave, I.N., 1984. Size-spectra and aggregation of suspended particles in the deep ocean. *Deep-Sea Research* **31**, 329-352.